Theoretical study of the excited states of the Kr* 2 excimer: Potential curves including a b i n i t i o spin–orbit coupling

E. Audouard and F. Spiegelmann

Citation: The Journal of Chemical Physics **94**, 6102 (1991); doi: 10.1063/1.460449
View online: http://dx.doi.org/10.1063/1.460449
View Table of Contents: http://scitation.aip.org/content/aip/journal/jcp/94/9?ver=pdfcov
Published by the AIP Publishing

Theoretical study of the excited states of the Kr_2^* excimer: Potential curves including *ab initio* spin–orbit coupling

E. Audouard
Laboratoire TSI, Equipe de Spectroscopie, CNRS, U.R.A. 842, Université Jean Monnet, 23, rue du docteur Paul Michelon, 42023 Saint-Etienne, Cedex, France

F. Spiegelmann
Laboratoire de Physique Quantique, CNRS, U.R.A. 505, Université Paul Sabatier, 118, route de Narbonne, 31062 Toulouse Cedex, France

(Received 14 November 1990; accepted 31 December 1990)

The potential energy curves for all the adiabatic Ω states dissociating into Kr + Kr, Kr + Kr*(5*s*,5*s*'), Kr + Kr*(5*p*), and some higher states are calculated using multireference perturbative CI algorithms (CIPSI/CIPSO) with relativistic averaged and spin–orbit core pseudopotentials. A partially diabatic representation of the potential curves rationalizes the complex features of the adiabatic states induced by numerous avoided crossings. A systematic comparison is carried out with extensive experimental data, including absorption from the ground state, fluorescence data, and transient absorption spectroscopy.

I. INTRODUCTION

Since the first estimations of Mulliken,[1-3] who predicted the general features of their electronic structure on the special case of Xe_2^*, rare gas excimers have been the object of continuous theoretical interest. Based on Mulliken's prescriptions, qualitative estimates of the potential energy curves were proposed by Barr *et al.*[4] for Kr_2^*, Lorents,[5] and also Chang and Setser[6] for Ar_2^*. The electronic structure of homonuclear excimers is well featured by an ionic molecular core and an electron in a diffuse Rydberg orbital. Without spin–orbit coupling, the electronic structure of the positive ion is characterized by the nature of the hole created in the valence molecular orbitals (MOs) of the dimer, yielding four states, namely $^2\Sigma_u^+$ (attractive), $^2\Pi_g$ and $^2\Pi_u$ (essentially nonbonding, except at large internuclear distance), and $^2\Sigma_g^+$ (very repulsive). The nature of the core parents determines the behaviors of the Rydberg states.

Following Mulliken's work, more quantitative investigations of the electronic properties were undertaken for most rare gas species. After the initial work of Cohen and Schneider on Ne_2^+,[7,8] Wadt[9,10] published a systematic *ab initio* study of the positive ions of all the heavier homonuclear dimers (Ar_2^+, Kr_2^+, and Xe_2^+) using frozen core all-electron (AE) configuration interaction (CI) calculations. Later, Wadt *et al.*,[11] Ermler *et al.*,[12] and Christiansen *et al.*[13] showed the ability of effective core potentials (EP) and averaged relativistic core potentials (AREP) to reproduce the AE results with a satisfactory accuracy. As concerns ions, one may also quote the local spin density calculation of Michels *et al.*[14] who carried out a systematic investigation of the series from Ne_2^+ to Xe_2^+.

The excited states of neutral systems also gave rise to numerous investigations. Studies for the lighter dimers could be performed using AE calculations. Apart from the special case of the He_2^* four-electron system which was originally investigated by Guberman and Goddard[15] using the generalized valence bond method, CI calculations were carried out for Ne + Ne* by Cohen and Schneider[7,8] [Ne*(3*s*) configuration], Iwata[16] [Ne*(3*s*) and Ne*(3*p*)], and Grein *et al.*[17-19] [Ne*(3*s*), Ne*(3*p*), and Ne*(4*s*)]. Saxon and Liu[20] also performed an AE-CI treatment of the lowest $^3\Sigma_u^+$ and $^3\Sigma_g^+$ states dissociating into Ar + Ar*(4*s*).

Most other CI studies on neutral excimers were achieved using the pseudopotentials or effective core potential approach, and more specifically, the formalism derived by Durand and Barthelat[21-22] and its relativistic extension given later by Teichteil *et al.*,[23] or independently, the procedure proposed by Ermler *et al.*[12] and Christiansen *et al.*[24] Ermler *et al.*[12] determined the potential energy curves of Xe_2^* dissociating into Xe + Xe*(6*s*). The Ar_2^* system was extensively studied, including states dissociating into Ar*(4*s*) and in some cases into Ar*(4*p*), by Spiegelmann and Malrieu,[25] Castex *et al.*,[26] Teichteil and Spiegelmann,[27] Yates *et al.*,[28] Spiegelmann and Gadéa,[29] and Mizukam and Nakatsuji.[33] Potential curves of the Kr_2^* excimer correlated with Kr + Kr*(5*s*) were determined by Gadéa *et al.*,[30] while higher states, not including spin–orbit coupling, were investigated in the work of Spiegelmann and Gadéa.[29] One should also mention calculations using simpler methods as in the work of Berman and Kaldor,[31] or the semiempirical study of Vallée *et al.*[32]

The inclusion of relativistic effects appears to be of increasing importance when going from neon to xenon. In molecular calculations, it is convenient to separate relativistic effects into the so-called averaged relativistic effects, including the mass term and the Darwin term and the spin–orbit coupling effect which is responsible for the splitting and the fine structure. This scheme gave rise to the definition of relativistic effective potentials (REP) and later averaged relativistic effective potentials (AREP). Most of those procedures[11,12,23,24] provide shape-consistent pseudopoten-

 0021-9606/91/096102-23$03.00

tials,[34] i.e., pseudopotentials which are meant to reproduce both the one-electron valence energies and the shapes of the orbitals in the valence region, and have been developed in the same general framework. They vary through technical differences, such as the origin of the AE atomic reference calculation used for generating the pseudopotential. While Christiansen *et al.*[24] directly use numerical Dirac–Fock calculations in the *j–j* coupling scheme, Teichteil *et al.* use a two-component approximation[35] of the Dirac equation and a *l–s* coupling scheme with analytical expansions of the wave functions.

This separation between averaged relativistic effects and spin–orbit effects makes possible the inclusion of averaged relativistic pseudopotentials in conventional CI algorithms which do not account for the fine structure.

This convenience has been widely used for rare gas excimers[25-30,33] and ions.[11-13] Spin–orbit coupling was generally incorporated afterwards, following the simple procedure of Cohen and Schneider[7] also used on ions by Wadt[9] and subsequent authors. According to this procedure, the total Hamiltonian H, consisting of a sum of the electrostatic part H^{el} and the spin–orbit operator H^{SO}

$$H = H^{el} + H^{SO}$$

is expressed in the basis of the adiabatic $\{\Lambda S\Sigma\}$ states in which H^{el} is diagonal. The H^{SO} matrix elements are transferred from the asymptotic limit and taken semiempirically from atomic data. The $\{\Omega\}$ states are easily obtained via the diagonalization of the $[H^{el} + H^{SO}]$ resulting matrices, which can decouple according to the different $\{\Omega\}$ manifolds. This scheme remains valid as long as the short distance character of the adiabatic $\{\Lambda S\Sigma\}$ states can be unambiguously related to a given atomic configuration. It breaks down whenever the adiabatic states experience strong configuration mixing, as is the case in avoided crossing situations, for instance (for which such an "atoms in molecule" scheme should be applied in a diabatic formulation).

The Cohen and Schneider scheme was thus extensively used for dimer positive ions for which the lowest states remain valence states correlated with the np^5 configuration. Reliable results could also be obtained for the lowest ungerade metastable states of neutral excimers dissociating into the $np^5(n+1)s$ atomic configuration, since the $\{\Lambda S\Sigma\}$ parent states $^3\Sigma_u^+$, $^1\Sigma_u^+$, $^3\Pi_u$, and $^1\Pi_u$ remain rather well separated or weakly coupled with higher states. One should mention that this situation is certainly no longer true for Xe_2^*, since the $6s'$ and $6p$ configuration already overlap on the atom. Even for the treatment of gerade states of the lighter excimers, the Cohen and Schneider scheme is certainly questionable since:

(i) the lowest $^3\Sigma_g^+$ and $^1\Sigma_g^+$ states are characterized by shallow wells at short internuclear distance followed by barriers. This peculiar shape was predicted by Mulliken[1-3] and explained in terms of strong configuration mixing involving the $np^5(n+1)s$ and $np^5(n+1)p$ configurations (see Sec. IV). This original feature was later exemplified and discussed with Ne_2^* (Ref. 7) and also appears for the heavier excimers;[25-30]

(ii) the situation is still complicated by the presence of attractive $^{3,1}\Pi_g$ states, also correlated with the $(n+1)p$ atomic configuration which are predissociated by the repulsive $^{3,1}\Pi_g$ states originating from the $(n+1)s$ manifold. The crossings are located very close to the minima of the upper $^{3,1}\Pi_g$ states and in the neighborhood of the $^{3,1}\Sigma_g^+$ states minima. However, in this second type of avoided crossing, the coupling is weak and the avoidance is extremely localized.

For the above reasons, the use of the Cohen and Schneider method as applied very recently[33] to the adiabatic states of Ar_2^* in the region of crossing between the $4s$ and $4p$ states is certainly questionable.

As one gets higher in the excited spectrum, such configuration mixing becomes the common rule since the number of avoided crossings is increased with the density of states. Calculations including spin–orbit coupling in a more sophisticated treatment are thus needed. Recently, Grein *et al.*[19] achieved a fully *ab initio* calculation of the Breit–Pauli Hamiltonian in the basis of all-electron multireference CI wave functions for $Ne + Ne^*(4s)$ at medium and large distance, and found, as expected in this range, little difference with previous results obtained with semiempirical spin–orbit coupling. For heavier elements, an alternative approach is provided by going beyond relativistic averaged pseudopotentials with specific spin–orbit pseudopotentials which have been extensively tested and reviewed recently by Balasubramanian.[36] Unexpectedly, the only attempt up to now to use spin–orbit pseudopotentials for rare gas excimers concerns, to our knowledge, the gerade states of the Ar_2^* dimer.[27]

In a previous work by one of us,[29] the $\{\Lambda S\Sigma\}$ potential energy curves of Kr_2^* dissociating into $Kr + Kr^*(5s,5p)$ and involving attractive states correlated with higher atomic configurations such as $Kr^*(4d,6s,6p)$ were computed using averaged relativistic pseudopotentials. However, fine structure was not included, and direct comparison with experiment was therefore very difficult. Some authors have tried to correlate those $\{\Lambda S\Sigma\}$ potentials with atomic states including fine structure. Such correlation may yield artifactual results, especially at large internuclear distance since the magnitude of spin–orbit coupling is larger than the intramultiplet separations. The situation is still worse in $Xe^* + Xe$. The present work is concerned with the theoretical determination of $\{\Omega\}$ states potential energy curves dissociating adiabatically into $Kr + Kr^*(5s,5s')$ and $Kr + Kr^*(5p)$ and is a contribution aimed at providing a more extensive and reliable description of the electronic structure of the heavier homonuclear rare gas excimers. It was stimulated by the various new data recently obtained, due to the progress of experimental techniques which are now able to explore a wider range of the rare gas excited spectrum.

As concerns the spectroscopy of Kr_2^*, the experimental situation can be summarized as follows. Since the early work of Tanaka[37] on the vacuum uv spectrum of van der Waals molecules, several groups[30,38,39] were concerned with the study of bound–bound or bound–free absorption spectra from the $(1)O_g^+$ $(4p^6\ ^1S_0)$ ground state towards the excited states of ungerade symmetry correlated with $Kr^*(5s,5s')$ and also with emission spectra[40] from these states. Fluorescence induced spectroscopy[41-44] yielded spectroscopic infor-

mation on the outer branch of the lowest fluorescent excimer states $(1)1_u$ $(5s[3/2]_2)$ and $(1)O_u^+$ $(5s[3/2]_1)$, the minima of which are located at short internuclear distance, and also of the $(2)O_u^+$ $(5s'[1/2]_1)$ state, which exhibits a smaller well located above the ground state van der Waals minimum. In the case of the two first excimer states, uv emission may originate from high vibrationally excited levels populated directly, or from relaxed vibrational levels populated through collisional processes. Transient absorption spectroscopy[45–53] probes higher electronically molecular species excited from the relaxed levels of $(1)1_u$ $(5s[3/2]_2)$, $(1)O_u^-$ $(5s[3/2]_1)$, or even $(1)O_u^+$ $(5s[1/2]_1)$ in the short distance range, typically around the equilibrium distance of their Kr_2^+ ground state $1(1/2)_u$ parent. Resonantly enhanced multiphoton ionization (REMPI) from the Kr_2 ground state allows the study of excimer states at larger internuclear distance around the van der Waals minimum of $(1)O_g^+$.[54,55] The two types of experiments previously mentioned provide information on gerade states. Many of these new results are difficult to interpret in the absence of any fine structure information on the electronic spectrum beyond the lowest excimer states.

Moreover, the knowledge of the $\{\Omega\}$ potential curves is also of significant interest for kinetic studies in order to understand the deactivation mechanisms of excited atoms[56] and to provide a consistent description of collisional and radiative decays leading to the formation of relaxed excimer states.[57] Such kinetic models are needed in particular for studying short internuclear distance spectroscopy, since transient absorption towards higher molecular Rydberg states arise from those relaxed excimer states (Rydberg–Rydberg transitions).

Section II provides a brief description of the method used for the present calculations (averaged relativistic and spin–orbit pseudopotentials, basis sets, multireference perturbative CI, and spin–orbit coupling). Section III is devoted to a calculation of Kr_2^+ valence states including *ab initio* pseudopotential spin–orbit coupling, and can be considered as a test since several previous calculations and extensive experimental data are available for almost all bound states. Results concerning the ground state and the excited states of the neutral excimer are given in Sec. IV, together with a qualitative diabatic analysis of the $\{\Omega\}$ states rationalizing the adiabatic spectrum which appears to be very intricate in some areas. Section V provides some review of experimental data examined in the light of the present results.

II. METHOD

Following Ref. 23, the electrostatic Hamiltonian

$$H^{\mathrm{el}} = \sum_{i\in\mathrm{val}} [h_i + U_i^{\mathrm{ps}}] + \frac{1}{2} \sum_{i,j\in\mathrm{val}}^{i\neq j} \frac{1}{r_{ij}}$$

only involves the valence electrons. The averaged relativistic pseudopotential is expressed in a semilocal expansion over the Legendre polynomials:

$$U_i^{\mathrm{ps}} = \sum_A^{\mathrm{atoms}} \left[-\frac{Z_A}{r_{Ai}} + \sum_l U_l^A(r_{Ai}) P_l \right].$$

The spin–orbit operator is a sum of one-electron pseudopotentials

$$H^{\mathrm{SO}} = \sum_{i\in\mathrm{val}} U_i^{\mathrm{SO}},$$

where U_i^{SO} is also expanded in semilocal form

$$U_i^{\mathrm{SO}} = \sum_A^{\mathrm{atoms}} \sum_{lj} U_{lj}^A(r_{Ai}) P_{lj}.$$

The averaged relativistic potentials used here for krypton are the same as those given in Ref. 30. The spin–orbit pseudopotential has been also given in a work concerned with the ArKr* exciplex.[58]

The Gaussian basis set on each atom is the $(9s10p4d/5s5p3d)$ used in a previous work on Kr_2^* without spin–orbit coupling.[29] We have added one f-type function with exponent 0.7, which was optimized in order to maximize the correlation energy of the atom in its ground state at the Möller–Plesset second order level (MP2).

The molecular orbitals (MOs) were determined through a restricted Hartree–Fock (RHF) Nesbet procedure with occupation numbers 2 for the $(1)\sigma_g 4s$ and $(1)\sigma_u 4s$ orbitals, 11/6 for $(2)\sigma_g 4p$, $(1)\Pi_u^x 4p$, $(1)\Pi_u^y 4p$, $(1)\Pi_g^y 4p$, $(1)\Pi_u^y 4p$, and $(2)\sigma_u 4p$. This procedure provides averaged MOs of the Kr_2^+ system. Of course, exact open-shell calculation could be used for Kr_2^+, since the four lowest states $^2\Sigma_u^+$, $^2\Pi_g$, $^2\Pi_u$, and $^2\Sigma_g^+$ have different symmetries. However, since we are essentially concerned with the neutral excimer, one needs to be able to describe on equal footing configurations of same symmetry which differ by the nature of the ionic core. It is clear that this MO set is not very well suited for the ground state which appears as a by-product of our calculation.

The potential energies of $\{\Lambda S\Sigma\}$ states (states without spin–orbit coupling) were determined using the multireference perturbative (CI) algorithm CIPSI[59] in its quasidegenerate perturbative theory (QDPT) formulation,[60] which has been shown to be suited for very degenerate situations, and especially in the case of numerous avoided crossings. A restricted diagonalization is performed within a generating multireference (MR) set S of N_S selected determinants $\{\phi_K\}$ which span the N relevant excited states $(N \leqslant N_S)$

$$P_S H^{\mathrm{el}} P_S |\psi_I^{(0)}\rangle = E_I^{(0)} |\psi_I^{(0)}\rangle \quad I = 1,N,$$

$$P_S = \sum_{K\in S} |\phi_K\rangle\langle\phi_K|,$$

and an effective Hamiltonian is computed up to the second order of perturbation theory according to the QDPT scheme, the hermiticized matrix elements of which are

$$H_{IJ}^{\mathrm{el}} = \langle\psi_I^{(0)}|H^{\mathrm{el}}|\psi_J^{(0)}\rangle + \sum_{K\notin S} \frac{\langle\psi_I^{(0)}|H^{\mathrm{el}}|\phi_K\rangle\langle\phi_K|H^{\mathrm{el}}|\psi_J^{(0)}\rangle}{\Delta E},$$

$$\Delta E^{-1} = 1/2\left[(e_I^{(0)} - e_K^{(0)})^{-1} + (e_J^{(0)} - e_K^{(0)})^{-1}\right].$$

The denominators are defined according to the barycentric Möller–Plesset definition. The diagonalization of the $[H_{IJ}^{\mathrm{el}}]$ matrix yields the adiabatic $\{\Lambda S\Sigma\}$ eigenstates and their corresponding potential energy values. The MR subspace S is

selected and augmented iteratively until no determinant in the first order contribution exceeds a given threshold $\tau = 0.05$. $\{\Omega\}$ potential energy curves are obtained from the diagonalization of the total Hamiltonian expressed in the basis of all the interacting $\{\Lambda S\Sigma\}$ states $\{\psi_I^{(0)}\}$ (including all relevant degenerate space and spin components) according to the CIPSO algorithm[23]

$$[H_{IJ}] = [H_{IJ}^{el}] + \langle\psi_I^{(0)}|H^{SO}|\psi_J^{(0)}\rangle.$$

In order to easily label the states, the Hamiltonian $[H_{IJ}]$ using a unitary transform is put into a bloc-diagonal form in the basis where the operator $\hat{J}_z = \hat{L}_z + \hat{S}_z$ is diagonal, allowing for the separation of fine structure states with different Ω values. The $+/-$ character for $\Omega = 0$ is assigned by checking the resulting overlaps of the calculated Ω states with reference symmetry vectors.

III. RESULTS FOR Kr_2^+

Kr_2^+ provides a relevant benchmack in order to probe the reliability of the present methodology since both AE[9] and AREP[13] calculations followed by semiempirical spin–orbit coupling, are available for the ion. Although the basis sets and the CI procedure are different from the ones used here, comparison with those previous calculations provides an opportunity to check both the averaged relativistic pseudopotentials and the spin–orbit pseudopotentials involved in the present work. Experimental information[55,61–64] is also rather extensive on the Kr_2^+ system.

Calculations at $R = 1000\,a_0$ were considered as providing asymptotic values. The $^2P_{1/2}$–$P_{3/2}$ splitting of the $4p^5$ configuration was found to be 5183 cm^{-1}, in fair agreement with the experimental value 5371 cm^{-1}.[65] The calculated ionization potential of krypton ($4p^6\ ^1S_0 \rightarrow 4p^5\ ^2P_{3/2}$) is 110 092 cm^{-1}, while the experimental value[65] is 112 915 cm^{-1}. This $\sim$2800 cm^{-1} error is essentially due to basis set incompleteness. Indeed, it was shown on the neon atom[66] that the limit of the correlation energy in a basis set with $l \leqslant 3$ was 0.320 Hartree instead of $\sim$0.380 Hartree[67] which is estimated to be the exact value (implying an error of the order of 10 000 cm^{-1}). Since the error in the correlation energy is certainly larger for the neutral atom than for the positive ion, one may expect a lack of correlation energy to yield an underestimation of the ionization potential, as obtained here. One may also expect this defect to be more serious for krypton since l-convergency generally gets worse when going from top to bottom in the periodic table.

As concerns the molecule, the $\{\Lambda S\Sigma\}$ states under consideration were the valence states of Kr_2^+, i.e., $^2\Sigma_u^+$, $^2\Pi_u^{x,y}$, $^2\Pi_g^{x,y}$, and $^2\Sigma_g^+$. The dimension of the final multireference space in each spin and space symmetry manifold was around 50. Since most bound excited states of the neutral molecule have a $^2\Sigma_u^+$ core, it is interesting to compare the $^2\Sigma_u^+$ potential energy curve obtained using the present pseudopotentials with the AREP result of Christiansen[13] *et al.* and with the AE calculation of Wadt[9] (Fig. 1). It is seen that both pseudopotential results are very close to the AE reference in the vicinity of the equilibrium distance; the AREP potential curve of Christiansen *et al.* being slightly more attractive than ours at longer distance.

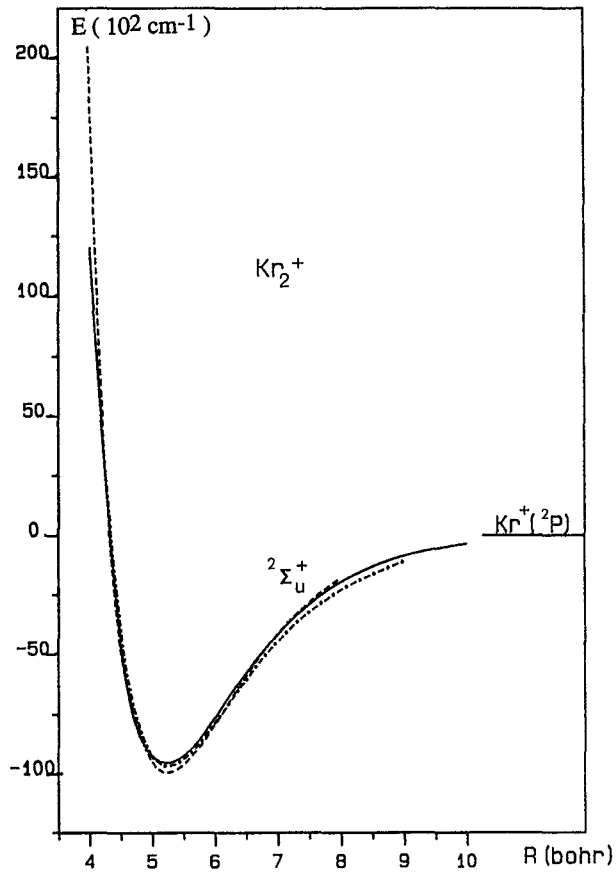

FIG. 1. Potential energy curves of the $^2\Sigma_u^+$ spin–orbit-less ground state of Kr_2^+. Full line: this work, averaged relativistic pseudopotentials; dashed line: all electron calculation of Wadt (Ref. 9); dashed–dotted line: AREP calculation of Christiansen *et al.* (Ref. 13).

More detailed comparison of the $\{\Omega\}$ potential curves can be made with the calculations of Wadt,[9] considering also experimental results. In the ungerade manifold (Fig. 2), the averaged difference between Wadt's results and ours is in the range $\sim$300 cm^{-1}, our ground state $1(1/2)_u$ ($^2\Sigma_{u1/2}^+$) being slightly less attractive ($D_0 = 8089\ cm^{-1}$) than the potential of Wadt ($D_0 = 8384\ cm^{-1}$). Both D_0 values seem to be underestimated with respect to experimental results which lie in the range 9300–9500 cm^{-1} (Table I). The inverse trend is observed for the $1(3/2)_u$ ($^2\Pi_{u3/2}$) and $2(1/2)_u$ ($^2\Pi_{u1/2}$) states which are a little more attractive than those of Wadt. In particular, the $1(3/2)_u$ potential curve of Wadt is always repulsive, while ours exhibits a very shallow well ($D_0 = 201\ cm^{-1}$ at $R_e = 7.67\ cm^{-1}$). Recently, Dehmer and Pratt[55] gave experimental evidence for the bound nature of this state, estimating D_0 to be 323 cm^{-1} (Table I). Similarly, our D_0 value for the $2(1/2)_u$ state ($D_0 = 863\ cm^{-1}$) is very close to the experimental value of Dehmer and Pratt ($D_0 = 887\ cm^{-1}$), while the value given by Wadt is slightly weaker ($D_0 = 776\ cm^{-1}$). As concerns the gerade manifold (Fig. 3), our potential curves are systematically slightly less repulsive than those of Wadt. The only bound state in this symmetry is $1(3/2)_g$ ($^2\Pi_{3/2g}$) for which our calculation gives $D_0 = 1368\ cm^{-1}$, while the result of Wadt is $D_0 \simeq 983$

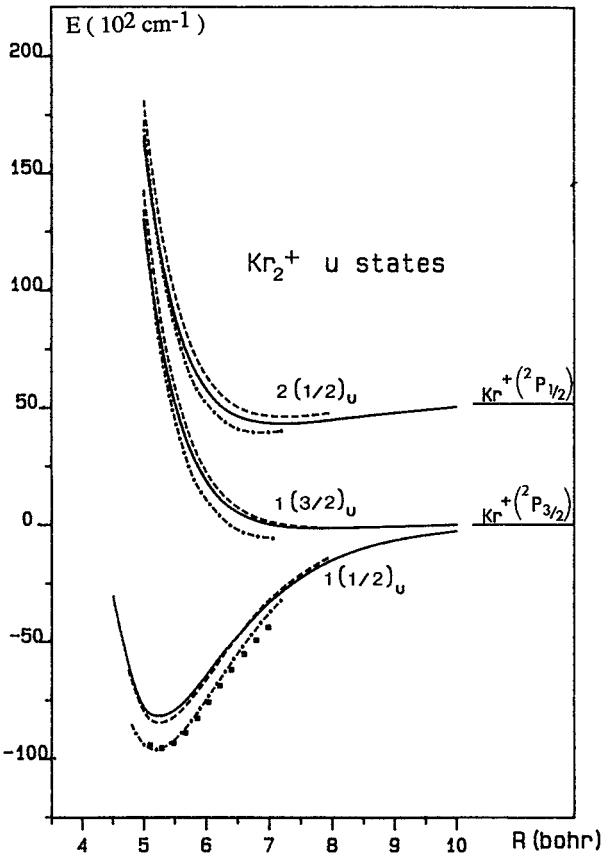

FIG. 2. Potential energy curves of Kr_2^+ ungerade states. Full line: this work; dashed line: Wadt (Ref. 9); dashed–dotted line: Michels *et al.* (Ref. 14); squares: Abouaf *et al.* (Ref. 63).

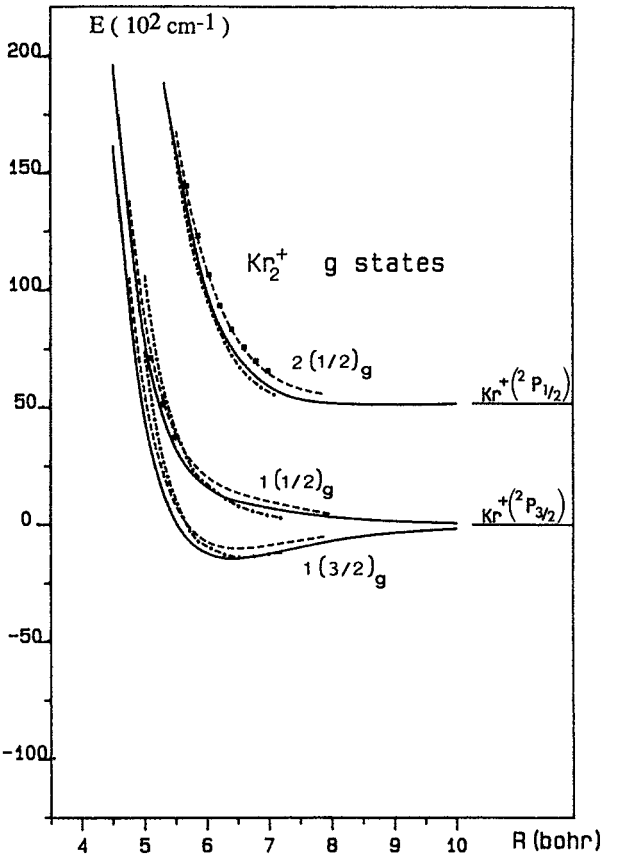

FIG. 3. Potential energy curves of Kr_2^+ gerade states. Full line: this work; dashed line: Wadt (Ref. 9); dashed–dotted line: Michels *et al.* (Ref. 14); squares: Abouaf *et al.* (Ref. 63).

TABLE I. Spectroscopic constants of Kr_2^+.

State	$R_e(a_0)$	$D_e(\text{cm}^{-1})$	$D_0(\text{cm}^{-1})$	$\omega_e(\text{cm}^{-1})$	Authors
$1(1/2)_u$					
			9279		Ng *et al.*[a]
			9489		Abouaf *et al.*[b]
			9279		Pratt and Dehmer[c]
	5.27	8472	8383	177	From Wadt[d]
	5.19	9618	9529	176.7	Michels *et al.*[e]
	5.24	8171	8089	165	This work
$1(3/2)_u$					
	Repulsive				Wadt[d]
	7.28	621	595	51.7	Michels *et al.*[e]
			323		Dehmer and Pratt[f]
	7.67	219	201	36	This work
$2(1/2)_u$					
	7.31	792	766	53	From Wadt[d]
			1130		Dehmer and Dehmer[g]
	6.87	1444	1409	70.2	Michels *et al.*[e]
			887		Dehmer and Pratt[f]
	7.20	888	863	51	This work
$1(3/2)_g$					
	6.48	1017	983	70	From Wadt[d]
			1291		Dehmer and Dehmer[g]
	6.58	1396	1357	78	Michels *et al.*[e]
			1291		Dehmer and Pratt[f]
	6.37	1411	1368	87	This work
$1(1/2)_g$	Repulsive				
$2(1/2)_g$	Repulsive				

[a] Reference 61. [c] Reference 64. [e] Reference 14. [g] Reference 62.
[b] Reference 63. [d] Reference 9. [f] Reference 55.

cm^{-1} and the experimental value obtained by Dehmer is $D_0 = 1291\ cm^{-1}$. It should be stressed that the experimental observations of Dehmer and Pratt are obtained using the REMPI-PES method. Since the neutral ground state is accurately known in the van der Waals region, those experimental results may be considered as rather accurate. Using photofragment spectroscopy data, Abouaf *et al.*[63] proposed estimated potential curves obtained by adjusting (shifting) Wadt's potentials in order to simulate their experimental results. They had to shift the $1(1/2)_u$ state downwards by $1113\ cm^{-1}$ (0.138 eV), which is consistent with the underestimations of the dissociation energy in Wadt's calculation and ours with respect to experimental results. As concerns the *g*-states their work could only probe the repulsive parts of the potentials. For the $1(1/2)_g$ ($^2\Pi_{1/2g}$), they estimated a potential lying between ours and the curve given by Wadt. For the $2(1/2)_g$ ($^2\Sigma^+_{1/2g}$), they almost kept the determination given by Wadt (0.001 eV shift) thus providing a more repulsive description than ours.

Theoretical results were also provided by Michels *et al.*[14] using the local density functional (LSD) approach and semiempirical spin–orbit coupling. Their results are systematically more attractive than ours in the medium internuclear distance range. In particular, they are likely to be in better agreement with experiment for the ground state. However, they seem to overestimate the dissociation energies of the other states (Table I). At short distance the trend is reversed and their potential curves tend to be more repulsive (especially in the *g* manifold) and it should be mentioned that the analycity (shape) of the LSD potential curves is fairly different from our results or those of Wadt.

IV. RESULTS FOR Kr_2

The selection criterion was kept the same for Kr_2 as for Kr_2^+ ($\tau = 0.05$). The lowest $\{\Lambda S\Sigma\}$ eigenstates in each symmetry manifold were considered in the calculation, i.e., 13 $^{1,3}\Sigma_g^+$ states [including the ground state (1) $^1\Sigma_g^+$], 12 $^{1,3}\Sigma_u^+$ states, 10 $^{1,3}\Pi_g$ states, 10 $^{1,3}\Pi_u$ states, 4 $^{1,3}\Delta_g$ states, 4 $^{1,3}\Delta_u$ states, 4 $^{1,3}\Sigma_g^-$ states, and 4 $^{1,3}\Sigma_u^-$ states. This includes all the $\{\Lambda S\Sigma\}$ eigenstates dissociating into $Kr(4p^6\ ^1S) + Kr(4p^6\ ^1S)$ and $Kr(4p^6\ ^1S) + Kr^*(5s, 5p)$ and also some higher states dissociating towards higher asymptotic limits as $Kr^*(4d, 6s,$ and $6p)$. Since the selection criterion for the multireference spaces had to be fulfilled simultaneously for all excited states, the sizes of those spaces were larger than in the Kr_2^+ case, i.e., around 100 determinants in each space and symmetry manifold. The number of determinants involved in the perturbation expansion generated by the MR subspace ran up to $\sim 4\times 10^6$ in the $^{3,1}\Sigma_g^+$, $^{3,1}\Sigma_u^+$, $^{3,1}\Pi_g$, and $^{3,1}\Pi_u$ manifolds, and about half for the $^{3,1}\Delta_g$, $^{3,1}\Delta_u$, $^{3,1}\Sigma_g^-$, and $^{3,1}\Sigma_u^-$ manifolds. The effective Hamiltonian was spanned over all space and spin $\{\Lambda S\Sigma\}$ eigenstates previously mentioned; the gerade and ungerade manifolds being treated independently. One should notice that the $5p'$, $4d$, $6s$, and $6p$ atomic fine structure terms strongly overlap. Since we did not include *all* the $\{\Lambda S\Sigma\}$ states dissociating into Kr^* ($4d$, $6s$, and $6p$), the coupling of $\{\Lambda S\Sigma\}$ states is uncomplete in this higher area of the spectrum and we have focused our attention on the lowest $\{\Omega\}$ roots dissociating into $Kr^*(5s, 5s',$ and $5p)$, although some higher states are obviously included in the present calculation.

Excited states experience multiple and successive avoided crossings, yielding rather complex adiabatic potential curves. According to Mulliken's arguments and the subsequent calculations of Spiegelmann and Gadéa[29] who analyzed spin–orbit-less electronic states, the essential features governing the excited states may be conveniently depicted by referring to configurations consisting of an ionic molecular core $^2\Lambda_{g,u}$ ($\Lambda = \Sigma^+, \Pi$) associated with a Rydberg molecular orbital $\lambda^*_{g,u}$ ($\lambda^* = \sigma,\pi,\delta\cdots$). For sake of understanding, it is convenient to adopt a diabatic point of view with respect to the excited molecular orbital (MO), the core being considered as treated adiabatically. The Rydberg MOs can be given a qualitative diabatic description if considered as properly symmetrized valence bond combinations of atomic orbitals (AOs) of the separated atoms. At finite internuclear distance, the Rydberg MOs are essentially characterized by their promoted vs unpromoted character as they transform into orbitals of the united atom. This character is directly related to their symmetry. Unpromoted MOs (respectively, promoted MOs) are gerade (respectively, ungerade) whenever they originate from orbitals of the separated atoms with even (respectively, odd) parity. Thus the relevant MOs in the short distance range are $\sigma_g ns$, $\sigma_u np$, $\pi_u np$, $\sigma_g nd$, $\pi_g nd$, and $\delta_g nd$. The association of a given core with one of these Rydberg MOs generates the possible diabatic states correlated with *ns*, *np*, and *nd* atomic excitations (see Table II). One can obtain easily a qualitative picture of the diabatic potential curves of excimers by drawing curves paralleling the ion curves and adequately correlated with the atomic configurations. This is equivalent to stating that the quantum defect is roughly the same for the molecular excimer and the atomic configuration into which it diabatically dissociates, as proposed in our previous theoretical paper in which this type of diabatic building of the states was introduced and sketched.[29] Recent transient absorption experiments by Conrad *et al.*,[68] who observed lines related to Rydberg series, tend to confirm such a description. It seems that, even at the excimer equilibrium distance ($R = 5.2\ a_0$), a labeling of the Rydberg MOs considering correlation with orbitals of separated atoms is to be preferred to a labeling considering correlation with orbitals of the united atom, since promotion is not fully achieved at least for the lowest excited states. Beyond this simple description, the behavior of the excited states is further determined by intraconfiguration interactions, interconfiguration interaction, and fine structure. Intraconfiguration interactions affect essentially the intermediate and long distance range ($R \geqslant 6\ a_0$ for krypton), where the molecular states transform into atomic states. At long internuclear distance, for instance, configurations $[^2\Lambda_u]\lambda^*_g$ and $[^2\Lambda_g]\lambda^*_u$ in the ungerade case, or $[^2\Lambda_u]\lambda^*_u$ and $[^2\Lambda_g]\lambda^*_g$ in the gerade case, tend to span the $\{\Lambda S\Sigma\}$ states with equal weights, because of angular momentum coupling rules. For the same reason, configurations of same total symmetry but with different Λ and λ can get coupled at long distance. Especially in the intermediate and long range, the excited states are strongly dependent on spin–orbit coupling.

TABLE II. Building of diabatic states from ionic core and unpromoted Rydberg orbitals. The core nature provides the repulsive or attractive behavior.

	$^2\Sigma_u^+$ (Attractive)	$^2\Pi_u$ (Moderately repulsive)	$^2\Pi_g$ (Moderately repulsive)	$^2\Sigma_g^+$ (Repulsive)
$\sigma_g ns$	$^{3,1}\Sigma_u$	$^{3,1}\Pi_u$	$^{3,1}\Pi_g$	$^{3,1}\Sigma_g^+$
$\sigma_u np$	$^{3,1}\Sigma_g^+$	$^{3,1}\Sigma_g$	$^{3,1}\Pi_u$	$^{3,1}\Sigma_u^+$
$\pi_u np$	$^{3,1}\Pi_g$	$^{3,1}\Sigma_g^+, ^{3,1}\Delta_g, ^{3,1}\Sigma_g^-$	$^{3,1}\Sigma_u^+, ^{3,1}\Delta_u, ^{3,1}\Sigma_u^-$	$^{3,1}\Pi_u$
$\sigma_g nd$	$^{3,1}\Sigma_u^+$	$^{3,1}\Pi_u$	$^{3,1}\Pi_g$	$^{3,1}\Sigma_g$
$\pi_g nd$	$^{3,1}\Pi_u$	$^{3,1}\Sigma_u^+, ^{3,1}\Delta_u, ^{3,1}\Sigma_u^-$	$^{3,1}\Sigma_g^+, ^{3,1}\Delta_g, ^{3,1}\Sigma_g^-$	$^{3,1}\Pi_g$
$\delta_g nd$	$^{3,1}\Delta_u$	$^{3,1}\Phi_u, ^{3,1}\Pi_u$	$^{3,1}\Phi_g, ^{3,1}\Pi_g$	$^{3,1}\Delta_g$

As concerns interconfiguration interactions, two cases are expected:

(i) The first case involves an upper attractive state with $^2\Sigma_u^+$ core and an essentially repulsive state with $^2\Pi_g$ or $^2\Pi_u$ core. Since the cores are different, such must be the Rydberg MOs because the global symmetry is the same. This is a case of bielectronic interaction which is generally small and the adiabatic avoidance is weak. There is not much difference between adiabatic and diabatic states, except at the crossing location, and the situation may be conveniently depicted in terms of diabatic states. A typical situation of this kind (see below) is the crossing between $^{3,1}\Pi_g$ states correlated with Kr*(5p) and those correlated with Kr*(5s) (attractive $[^2\Sigma_u^+]\pi_u 5p$ configuration vs repulsive $[^2\Pi_g]\sigma_g 5s$ configuration).

(ii) The second case is more intricate. It occurs for a crossing between an attractive state with $^2\Sigma_u^+$ core, i.e., $[^2\Sigma_u^+]\lambda^{**}_{g,u}$ and a lower state with $^2\Sigma_g^+$ core, which is in principle very repulsive, i.e., $[^2\Sigma_g^+]\lambda^{*}_{u,g}$. However, at intermediate distance, the asymptotically degenerate $[^2\Sigma_u^+]\lambda^{*}_{g,u}$ configuration still has a large weight in the lowest state wave function. It has the same core as the upper state and orbital $\lambda^{*}_{g,u}$ shows a strong overlap with $\lambda^{**}_{g,u}$, inducing a very strong coupling between the two interacting states. As a result, the lowest adiabatic state usually exhibits a peculiar feature consisting of a well at short internuclear distance followed by a barrier to dissociation, while the upper state looses any bound character. For such states, diabatic correlation can still be used in order to compare, analyze, and assign short distance Rydberg series; however, the following of the potential curves with the distance is more adequate in terms of the adiabatic description, due to the magnitude of the coupling and the nonlocal character of the avoided crossing. This feature was predicted by Mulliken,[1-3] and analyzed in terms of orbital promotion. A typical situation is met by the lowest $(1)^3\Sigma_g^+(5s\,^3P)$ and $(2)^1\Sigma_g^+(5s\,^1P)$ states of krypton and of other excimers.[25-30]

Although spin–orbit coupling is significant in krypton and somewhat complicates the electronic structure (avoided crossings due to spin–orbit interaction, for instance), the $\{\Omega\}$ states still remember the structure of their $\{\Lambda S\Sigma\}$ parents at least in the short distance range where the main features of the above description can still be identified. The $\{\Omega\}$ components are obtained from $\{\Lambda S\Sigma\}$ parents according to the following generation rules:

$$^1\Sigma^+ \rightarrow O^+,$$
$$^3\Sigma^+ \rightarrow 1, O^-,$$
$$^1\Pi \rightarrow 1,$$
$$^3\Pi \rightarrow 2,1, O^+,\ O^-$$
$$^1\Sigma^- \rightarrow O^-,$$
$$^3\Sigma^- \rightarrow 1, O^+,$$
$$^1\Delta \rightarrow 2,$$
$$^3\Delta \rightarrow 3,2,1.$$

The arguments developed in the present section will be used in order to discuss and understand the qualitative behavior of the calculated $\{\Omega\}$ states which are presented in the following. In order to provide a convenient support for the discussion, diabatic potentials are also given. They were obtained by analyzing the content of the calculated adiabatic wave functions and reassigning diabatically the potential values away from the avoidance areas. Only short distance interconfiguration crossings [cf. type (i)] (characterized by bielectronic coupling) have been restored while neither medium distance strongly avoided crossings [corresponding to type (ii)] nor intermediate and intraconfiguration long range avoided crossings (either electronic or due to spin–orbit) have been restored. This procedure is of course arbitrary. However, it provides a general understanding of the complex shapes characterizing the adiabatic states. Moreover, in the areas of interconfiguration crossings and whenever the coupling is weak, bound diabatic upper states predissociated by repulsive states might provide a more relevant picture than the adiabatic representation, since the Born–Oppenheimer approximation breaks down. Thus the spectroscopic characterizations of the diabatic states are also given in order to complement data corresponding to the adiabatic results. $\{\Lambda S\Sigma\}$ potential curves before spin–orbit

coupling show no significant difference with the results given in a previous work,[29] the addition of extra f functions in the present work providing only small quantitative differences. Thus, only numerical results corresponding to $\{\Omega\}$ states are given. In the following, adiabatic states are labeled with arabic numerals, while diabatic states are labeled with roman numerals.

A. Asymptotic transitions

As for Kr_2^+, the energy values at $R = 1000\,a_0$ were considered as reference asymptotic values. When several Ω states dissociate into degenerate atomic states, the asymptotic transition energies were taken as the averaged of the corresponding states in the different symmetry manifolds. Those transitions are listed in Table III and compared with the experimental values of Moore.[65] Calculated transition energies from the ground states exhibit a systematic underestimation of 2500 ± 150 cm^{-1}. This error is obviously related to the 2800 cm^{-1} error on the ionization potential, and corresponds to the correlation error on the ionic core of the Rydberg states. This error is slightly smaller due to the presence of the Rydberg electron. Apart from this systematic error, it is clear in Table III that the intra- and intermultiplet separations are obtained with an averaged error less than 150 cm^{-1}. This correct calculation of the atomic spectrum is of importance for the location of the avoided crossings experienced by molecular states correlated with the asymptotes under consideration in the present work.

B. The ground state (1) O_g^+(Kr, $4p^6\ ^1S_0$)

Although the Nesbet MOs used in the present calculation are not suited for the closed-shell ground state, this defect should be partly compensated in the CI process due to the inclusion of single excitations in the multireference space or in the perturbation. Better accuracy could certainly be obtained with a specific calculation of the ground state, also including basis set superposition error (BSSE). However, the present determination is consistent with the calculations of the excited states and will enable us to discuss absorption and fluorescence spectra. The $(1)O_g^+$ ground state discussed here is the first root of the effective Hamiltonian (including SO coupling) corresponding to the O_g^+ manifold.

TABLE III. Asymptotic transitions energies (cm^{-1}) for krypton. The last column is obtained by a 2500 cm^{-1} (averaged error) shift from the calculated transitions. Experimental values are taken from Moore (Ref. 65).

Racah notation	Russel–Saunders notation	Experimental	Calculated	Error	Calculated with shift
$5s[3/2]_2$	$^3P_2$	79 972	77 511	2461	80 011
$5s[3/2]_1$	$^3P_1$	80 916	78 532	2354	81 032
$5s'[1/2]_0$	$^3P_0$	85 192	82 542	2650	85 042
$5s'[1/2]_1$	$^1P_1$	85 847	83 302	2545	85 802
$5p[1/2]_1$	$^3S_1$	91 169	88 539	2630	91 039
$5p[5/2]_3$	$^3D_3$	92 295	89 781	2527	92 281
$5p[5/2]_2$	$^3D_2$	92 308	89 862	2446	92 362
$5p[3/2]_1$	$^3D_1$	92 965	90 547	2418	93 047
$5p[3/2]_2$	$^1D_2$	93 124	90 678	2446	93 178
$5p[1/2]_0$	$^3P_0$	94 094	91 598	2496	94 098

The van der Waals range of the potential curve is illustrated in Fig. 4. The calculated characteristics are $R_e = 7.84$ bohr, $D_e = 250$ cm^{-1}, $\omega_e = 23$ cm^{-1}, while the accurate HFD-C multiproperty fit of Aziz[69] yields $R_e = 7.58$ bohr, $D_e = 139$ cm^{-1}, $\omega_e = 21$ cm^{-1}. This 110 overestimation of the dissociation energy is certainly to be attributed to BSSE and to the use of inadequate MOs. Accurate potentials for van der Waals systems are anyway very tedious to calculate, and one may quote, for instance, the recent work of Krauss *et al.*[70] who added the repulsive self-consistent field (SCF) energy to a multipole expansion for the dispersion energy (thus avoiding the noise in the intra-atomic correlation energy) and obtained $R_e = 7.94$ bohr and $D_e = 112.9$ cm^{-1}.

Alternatively, the repulsive portion of the calculated potential curve (Fig. 5) is in fairly good agreement with the potential of Aziz. At $R = 5.2\,a_0$ (which is the relevant range in fluorescence experiments) our potential lies slightly above Aziz' curve by 600 cm^{-1}. One should mention, however, that another curve was proposed by Foreman, Lee, and Rol[71] and later slightly modified by Barzen *et al.*[43] It is much more attractive and lies 1600 cm^{-1} below our's at $R = 5.2$ bohr.

C. The ungerade excited states

The u states are displayed in Figs. 6(a)–10(a) and their spectroscopic constants are listed in Tables IV–VII. We first discuss the states generated by the first atomic configuration

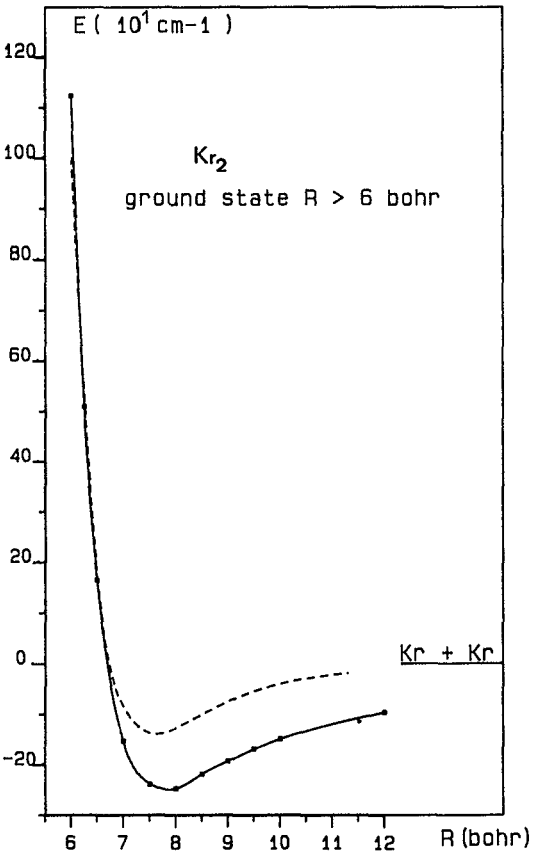

FIG. 4. Potential energy curve of the $(1)O_g^+$ ground state of Kr_2 for $R > 6$ bohr. Full line: this work; dashed line: Aziz (Ref. 69).

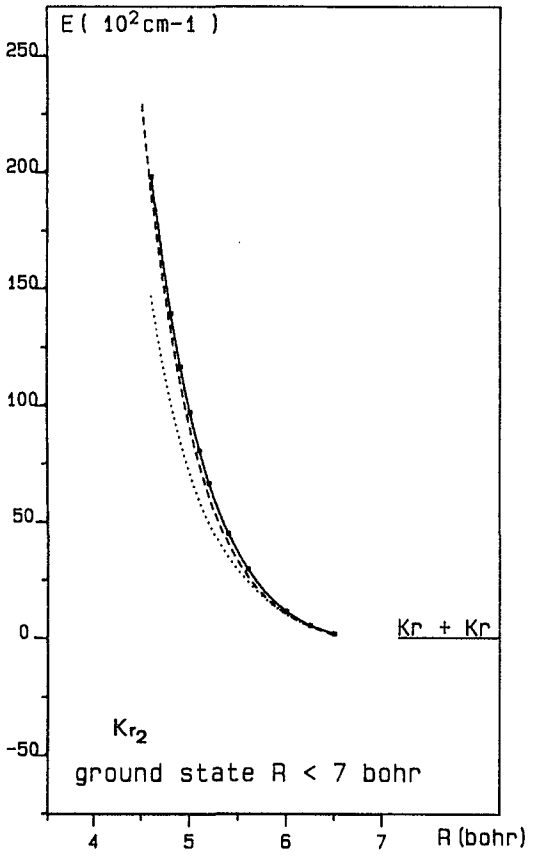

FIG. 5. Potential energy curve of the $(1)O_g^+$ ground state of Kr_2 for $R < 7$ bohr. Full line: this work; dashed line: Aziz (Ref. 69); dotted line: Foreman *et al.* (Ref. 71) (see also Barzen *et al.*, Ref. 43).

with one electron in a $5s$ orbital. Without spin–orbit coupling, the atomic states $5s\,^3P$ and $5s\,^1P$ give rise to two attractive states, $(1)^3\Sigma_u^+$ and $(1)^1\Sigma_u^+$, characterized by the $[^2\Sigma_u^+]\sigma_g 5s$ configuration, and two repulsive states $(1)^3\Pi_u$ and $(1)^1\Pi_u$, characterized by the $[^2\Pi_u]\sigma_g 5s$ configuration. When spin–orbit is included, one obtains three attractive states at short internuclear distance (around $R = 5.2\ a_0$), namely $(1)O_u^-(5s[3/2]_2)$ and $(1)1_u\ (5s[3/2]_2)$, almost degenerate and essentially spanned by $(1)^3\Sigma_u^+$, while $(1)O_u^+\ (5s[3/2]_1)$ has its larger component on $(1)^1\Sigma_u^+$. The dissociation energies of these bound states are hardly larger than in the previous calculation by Gadéa *et al.*[30] without f orbitals and semiempirical spin–orbit coupling. The repulsive $(1)^3\Pi_u$ and $(1)^1\Pi_u$ states generate two 1_u states, one O_u^- state, one O_u^+ state and one 2_u state [purely $(1)^3\Pi_u$], all of them being fairly repulsive if considered diabatically [Figs. 6(b)–10(b)]. At short distance, they cross attractive states diabatically dissociating into higher atomic configurations. The $(2)O_u^+\ (5s'[1/2]_1)$ state exhibits a shallow well which is specifically due to spin–orbit coupling, with a dissociation energy very close to the value obtained by Gadéa *et al.*[30]

The $5p$ atomic configuration is characterized before spin–orbit coupling by six states, namely ^3S, ^3D, ^1D, ^3P, ^1P, and ^1S. In the $^{3,1}\Sigma_u^+$ manifold, configurations $[^2\Sigma_g^+]\sigma_u 5p$ and $[^2\Pi_g]\pi_u 5p$ are diabatically repulsive, like the $^{3,1}\Pi_u$ states characterized by configurations $[^2\Pi_g]\sigma_u 5p$ and $[^2\Sigma_g^+]\pi_u 5p$. The $^{3,1}\Delta_u$ and $^{3,1}\Sigma_u^-$ states built on configuration $[^2\Pi_g]\pi_u 5p$ are weakly bound. Thus there is no strongly attractive ungerade state with $^2\Sigma_u^+$ core which at short distance is diabatically correlated with the $5p$ configuration. However, the $5p$ states exhibit interactions with attractive configurations having $[^2\Sigma_u^+]$ cores dissociating into higher asymptotes, namely $[^2\Sigma_u^+]\sigma_g 4d$ and $[^2\Sigma_u^+]\sigma_g 6s$ (two $^3\Sigma_u^+$ and two $^1\Sigma_u^+$ states), $[^2\Sigma_u^+]\pi_g 4d$ (one $^3\Pi_u$ state and one $^1\Pi_u$ state), $[^2\Sigma_u^+]\delta_g 4d$ (one $^3\Delta_u$ state and one $^1\Delta_u$ state). In the diabatic representation, one thus expects three O_u^+ states (III, IV, and V), three O_u^- states (III, IV, and V), five 1_u states (IV, V, VI, VII, and VIII), three 2_u states (III, IV, and V), and one 3_u state which all should exhibit attractive $^2\Sigma_u^+$ core character at short internuclear distance. This situation is illustrated on the diabatic pictures of the potential curves. As a consequence, the resulting adiabatic potential curves experience multiple interconfiguration avoided crossings and some states have several minima.

D. The gerade excited states

A similar analysis can be achieved for the g states [see Figs. 11(a)–14(a) and 15 for the adiabatic states and Figs. 11(b)–14(b) for the diabatic states]. As concerns the $5s$ asymptote, diabatic states $^{3,1}\Pi_g$ are built on configurations $[^2\Pi_g]\sigma_g 5s$ and are therefore nonbonding. The lowest $^{3,1}\Sigma_g^+$ states have the previously mentioned shape characterized by a shallow well followed by a barrier, due to a strong interaction with $^{3,1}\Sigma_g^+$ states dissociating into the $5p$ configuration. After spin–orbit coupling, the bound character almost disappears and only inflections still subsist in the potential curves [diabatic states $(II)O_g^-$, $(II)O_g^+$, $(II)1_g$ and $(III)1_g$]. All the Ω states are essentially repulsive. One may notice an intraconfiguration avoided crossing due to spin–orbit coupling between $(1)1_g(5s[3/2]_2)$ and $(2)1_g$ $(5s[3/2]_1)$. As concerns the $5p$ configuration, the $^{3,1}\Sigma_g^+$ states, built on configurations $[^2\Sigma_u^+]\sigma_u 5p$ are repulsive due to their strong interaction with the lowest states of same symmetry, while states $^{3,1}\Pi_g$ correspond to the $[^2\Sigma_u^+]\pi_u 5p$ configuration, and are strongly attractive. This attractive configuration is responsible for the important interconfiguration crossings between the $5s$, $5s'$, and $5p$ manifolds, which is a case of weak coupling. It generates the Ω diabatic states $(III)O_g^+$, $(III)O_g^-$, $(IV)1_g$, $(V)1_g$, and $(II)2_g$. In the O_g^- manifold and in the 1_g manifold, intraconfiguration avoided crossings occur at intermediate distance, also due to spin–orbit coupling, creating shallow wells in the upper states $(IV)O_g^-$ and $(VII)1_g$. Again, the adiabatic states exhibit multiple avoided crossings. Their spectroscopic constants are listed in Tables IX–XII.

V. DISCUSSION

The scope of this section is to survey and discuss the various experimental results with the help of the actual $\{\Omega\}$ potentials obtained in the previous section. The experimental data are examined in the following order: absorption from the ground state, fluorescence data, and transient absorption.

In the whole section, calculated transitions from and to

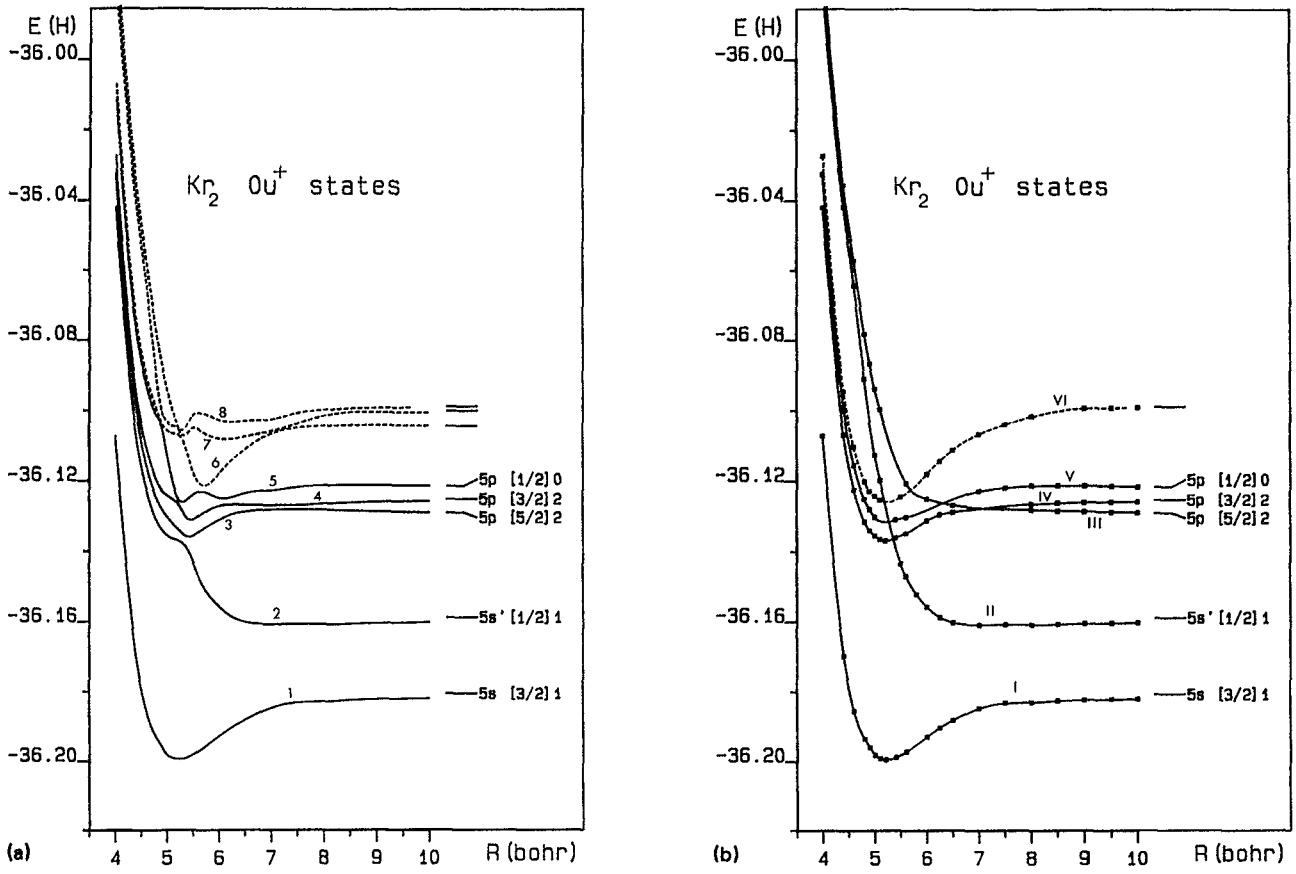

FIG. 6. Potential energy curves of the excited O_u^+ states of Kr_2^*. (a) adiabatic states; (b) diabatic states (the squares indicate the calculated potential values which were conserved for drawing the diabatic potentials). The dashed lines refer to potentials dissociating adiabatically higher than Kr*(5*p*).

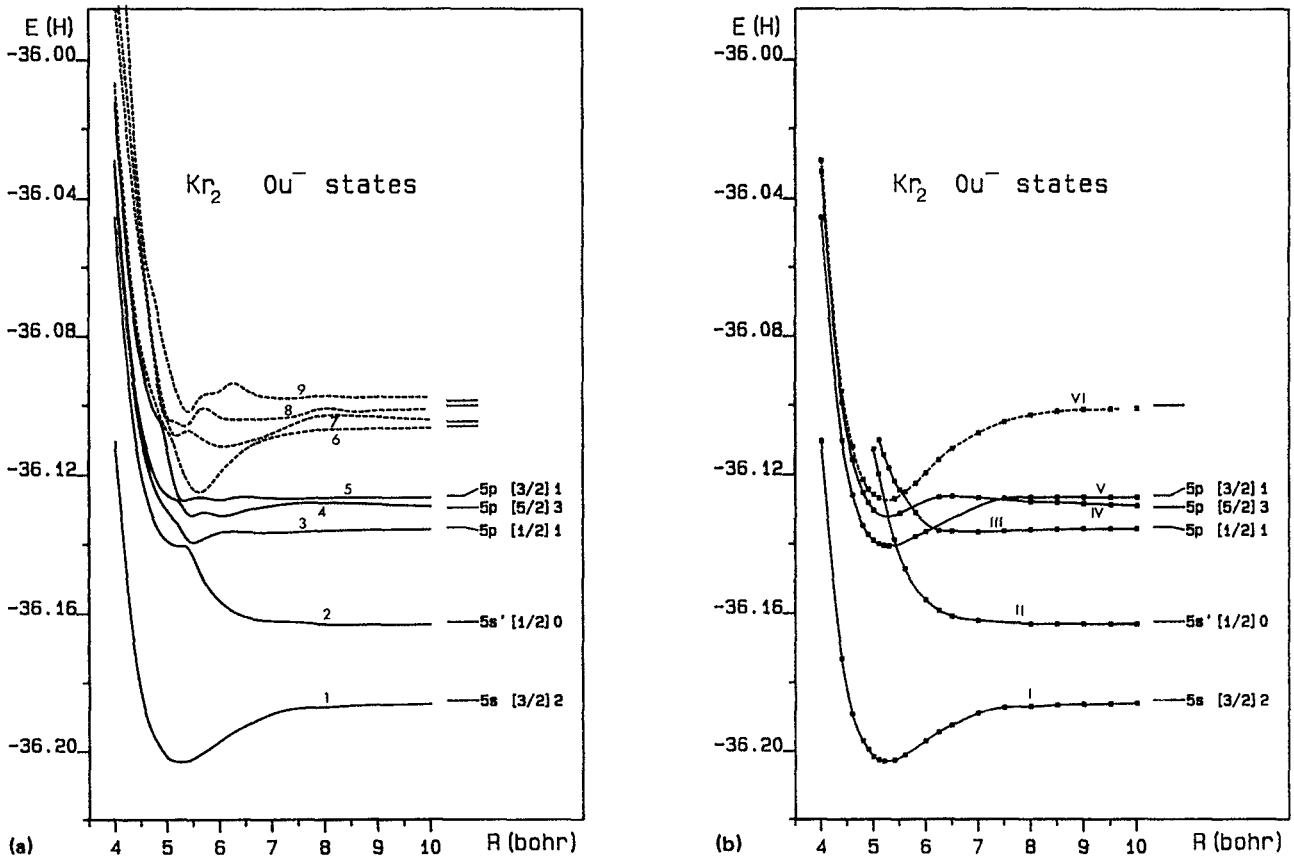

FIG. 7. Potential energy curves of the excited O_u^- states of Kr_2^*. (a) adiabatic states; (b) diabatic states (the squares indicate the calculated potential values which were conserved for drawing the diabatic potentials). The dashed lines refer to potentials dissociating adiabatically higher than Kr*(5*p*).

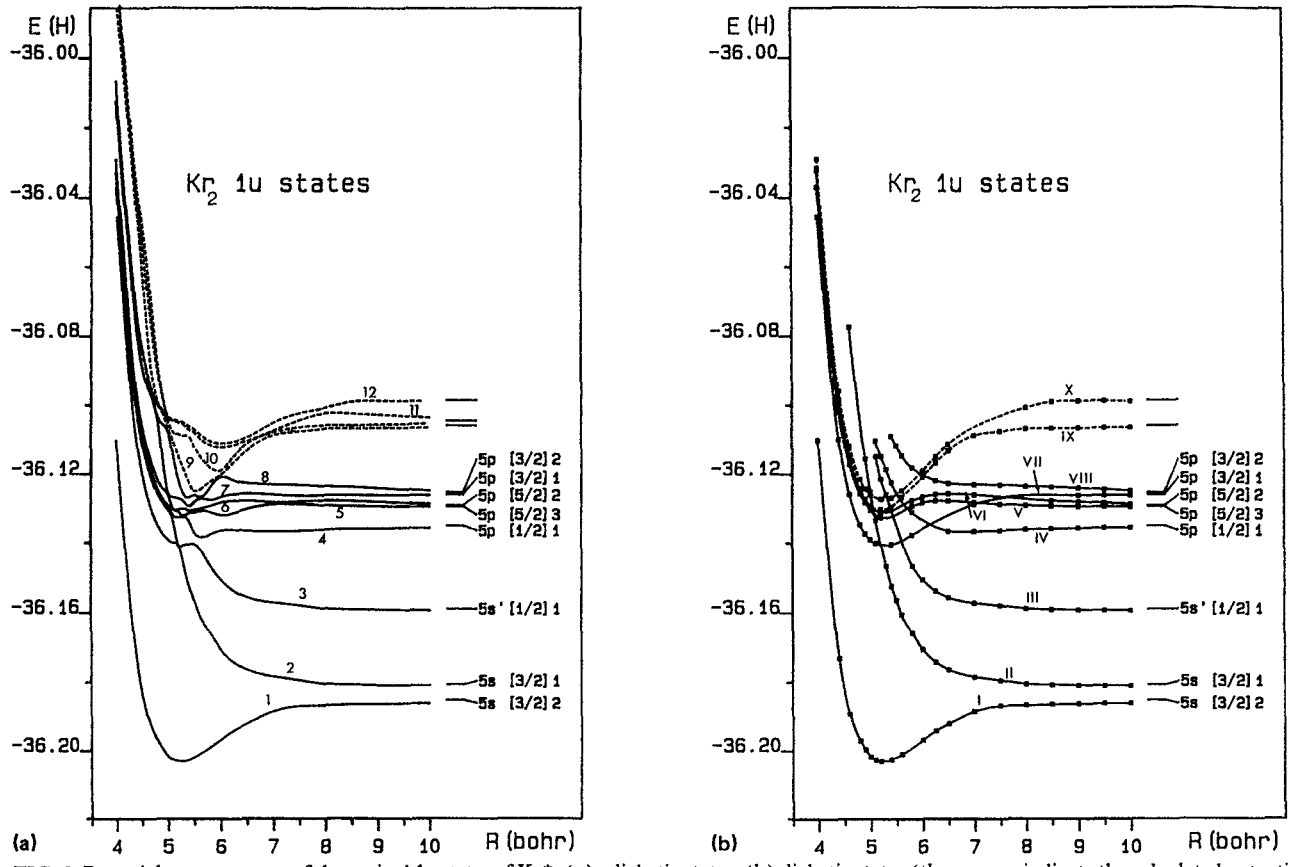

FIG. 8. Potential energy curves of the excited 1_u states of Kr_2^*. (a) adiabatic states; (b) diabatic states (the squares indicate the calculated potential values which were conserved for drawing the diabatic potentials). The dashed lines refer to potentials dissociating adiabatically higher than Kr*(5*p*).

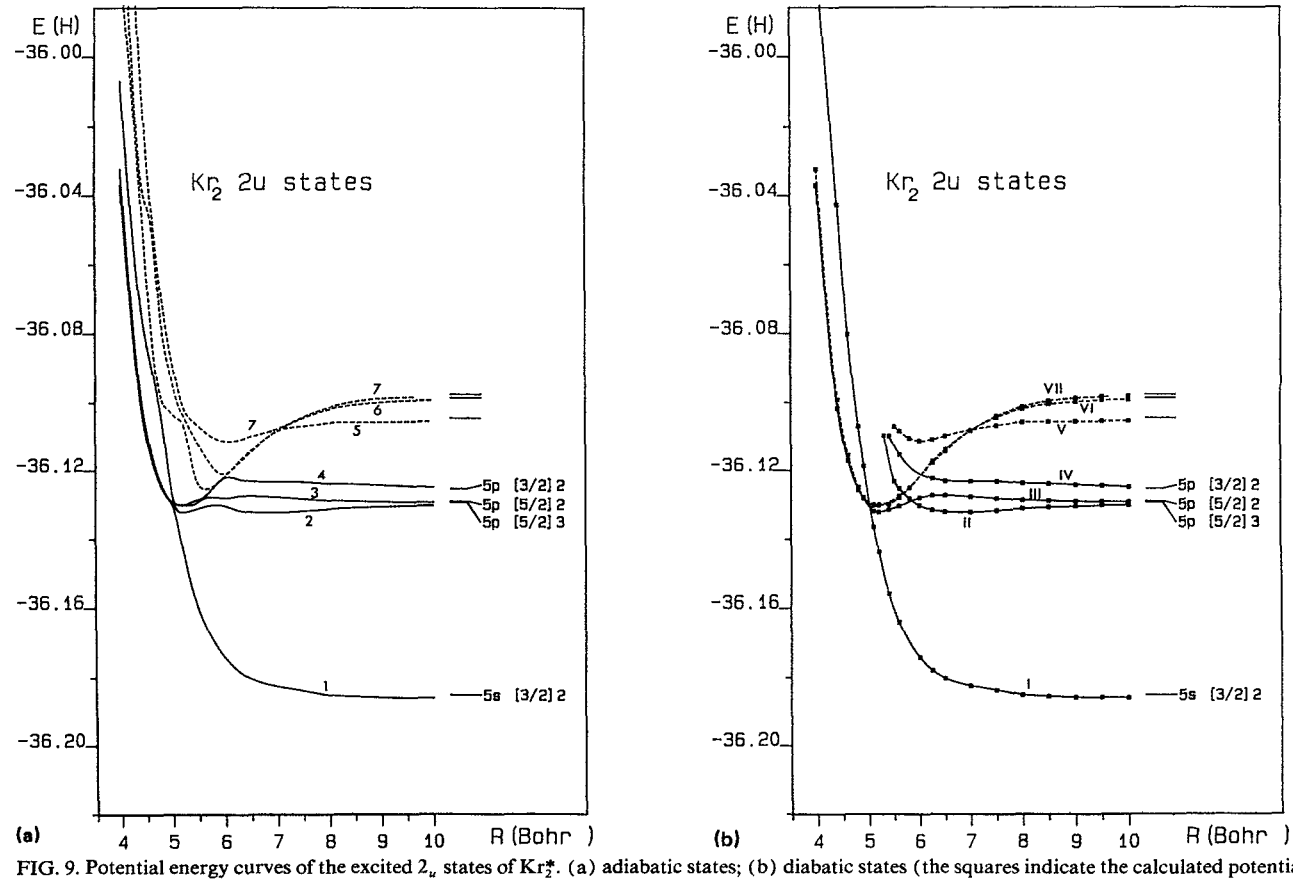

FIG. 9. Potential energy curves of the excited 2_u states of Kr_2^*. (a) adiabatic states; (b) diabatic states (the squares indicate the calculated potential values which were conserved for drawing the diabatic potentials). The dashed lines refer to potentials dissociating adiabatically higher than Kr*(5*p*).

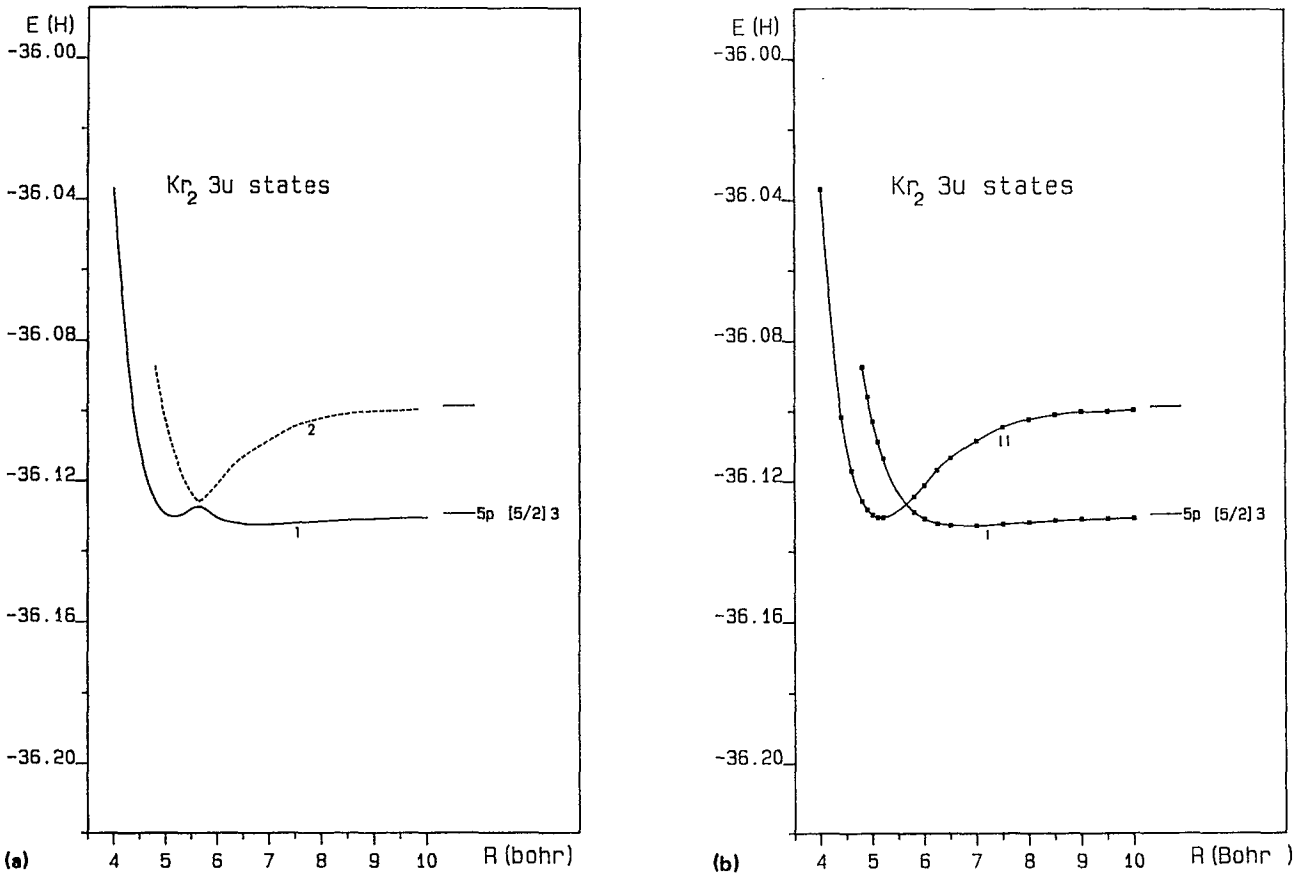

FIG. 10. Potential energy curves of the excited 3_u states of Kr_2^*. (a) adiabatic states; (b) diabatic states (the squares indicate the calculated potential values which were conserved for drawing the diabatic potentials). The dashed lines refer to potentials dissociating adiabatically higher than Kr*(5*p*).

the ground state are shifted ("corrected") by the systematic asymptotic error 2500 cm^{-1}.

A. Absorption from the ground state

This class of experiments provides information about the upper states around the equilibrium distance of the $(1)O_g^+$ ground state either of ungerade symmetry when a single photon is absorbed, or of gerade symmetry when two photons are absorbed.

1. Ungerade states

As concerns one-photon spectra, the high-resolution results of Tanaka[37] consist of three band systems (labeled I–III) assigned, respectively, to states $(1)1_u$ $(5s[3/2]_2)$, $(1)O_u^+$ $(5s[3/2]_1)$, and $(2)O_u^+$ $(5s'[1/2]_1)$ correlated with Kr* (5*s*, 5*s*′) and four systems (IV, V, VI, and VII) due to absorption by ungerade states dissociating into the 5*p* configuration. Complementary results about ungerade 5*s* and 5*s*′ states were obtained later by Gerardo and Johnson,[38]

TABLE IV. Spectroscopic constants of O_u^+ states.

State	Dissociation	Minima	$R_e(a_0)$	$D_e(cm^{-1})$	$\omega_e(cm^{-1})$
Adiabatic					
1	$5s[3/2]_1$	1	5.22	4137	173
2	$5s'[1/2]_1$	1	6.94	458	50
3	$5p[5/2]_2$	1	5.42	1567	285
4	$5p[3/2]_2$	1	5.46	1311	327
		2	7.26	379	27
5	$5p[1/2]_0$	1	5.30	1065	379
		2	6.08	828	155
Diabatic					
I	$5s[3/2]_1$	1	5.22	4137	173
II	$5s'[1/2]_1$	1	6.93	459	51
III	$5s[5/2]_2$	Repulsive			
IV	$5p[3/2]_2$	1	5.21	2578	232
V	$5p[1/2]_0$	1	5.19	2218	184
VI		1	5.24	5958	183

TABLE V. Spectroscopic constants of O_u^- states. Negative dissociation energies refer to minima above the asymptote.

State	Dissociation	Minima	$R_e(a_0)$	$D_e(cm^{-1})$	$\omega_e(cm^{-1})$
Adiabatic					
1	$5s[3/2]_2$	1	5.25	3943	158
2	$5s'[1/2]_0$	1	5.21	−4764	227
3	$5p[1/2]_1$	1	5.49	988	269
		2	6.85	349	35
4	$5p[5/2]_3$	1	5.46	530	311
		2	6.04	545	149
5	$5p[3/2]_1$	1	5.31	352	345
		2	5.98	299	154
		3	7.38	217	42
Diabatic					
I	$5s[3/2]_2$	1	5.25	3943	158
II	$5s'[1/2]_0$	Repulsive			
III	$5p[1/2]_1$	1	6.85	349	35
IV	$5p[5/2]_3$	1	5.24	659	178
V	$5p[3/2]_1$	1	5.30	3261	155
VI		1	5.27	6051	183

Laporte and Damany,[39] and particularly in the rather exhaustive study of Gadéa *et al.*[30] From the temperature dependence of the absorption profiles, Gadéa *et al.* could derive portions of the potential curves of both attractive and repulsive potentials in the distance range $7\,a_0 \leqslant R \leqslant 8.5\,a_0$ (3.7 Å $\leqslant R \leqslant$ 4.5 Å). In the same work, a rather extensive comparison was achieved with theoretical results obtained from CI calculations and semiempirical treatment of spin–orbit cou-

TABLE VI. Spectroscopic constants of 1_u states. Negative dissociation energies refer to minima above the asymptote. Values with a star (*) correspond to minima on the adiabatic curves which are very close to an avoided crossing and may have poor physical meaning.

State	Dissociation	Minima	$R_e(a_0)$	$D_e(cm^{-1})$	$\omega_e(cm^{-1})$
Adiabatic					
1	$5s[3/2]_2$	1	5.24	3928	163
2	$5s[3/2]_1$	Repulsive			
3	$5s'[1/2]_1$	1	5.25	−3896	463(*)
4	$5p[1/2]_1$	1	5.18	−523	268(*)
		2	5.65	769	247
		3	6.82	378	33
5	$5p[5/2]_3$	1	5.30	637	506(*)
		3	6.04	579	161
6	$5p[5/2]_2$	1	5.15	331	459(*)
		2	5.42	358	269(*)
		3	7.07	−173	58
7	$5p[3/2]_1$	1	5.41	771	520(*)
		2	5.81	352	239(*)
		3	7.48	88	45
8	$5p[3/2]_2$	1	5.38	365	433(*)
		2	5.62	316	387(*)
Diabatic					
I	$5s[3/2]_2$	1	5.24	3928	163
II	$5s[3/2]_1$	Repulsive			
III	$5s'[1/2]_1$	Repulsive			
IV	$5p[1/2]_1$	1	6.72	419	72
V	$5p[5/2]_3$	1	5.27	751	179
VI	$5p[5/2]_2$	1	5.24	455	174
VII	$5p[3/2]_1$	1	5.28	3259	148
VIII	$5p[3/2]_2$	Repulsive			
IX		1	5.19	5329	124
X		1	5.27	6309	152

TABLE VII. Spectroscopic constants of 2_u states. Negative dissociation energies refer to minima above the asymptote. Values with a star (*) correspond to minima on the adiabatic curves which are very close to an avoided crossing and may have poor physical meaning.

State	Dissociation	Minima	$R_e(a_0)$	$D_e(\text{cm}^{-1})$	$\omega_e(\text{cm}^{-1})$
Adiabatic					
1	$5s[3/2]_2$	Repulsive			
2	$5p[5/2]_3$	1	5.16	652	297.0(*)
		2	6.79	662	41
3	$5p[5/2]_2$	1	5.16	276	136
		2	5.99	−215	151
4	$5p[3/2]_2$	1	5.17	1057	193
		2	6.78	−437	41
Diabatic					
I	$5s[3/2]_2$	Repulsive			
II	$5p[5/2]_3$	1	6.76	667	46
III	$5p[5/2]_2$	1	5.18	704	202
IV	$5p[3/2]_2$	1	6.75	−430	50
V		1	6.04	1502	120
VI		1	5.16	6956	124
VII		1	5.17	7138	151

pling. The present results are in good agreement with the previous studies. The $v''=0\rightarrow v'$ (v' is a high vibrational number of the upper state) transitions observed by Tanaka are 79 851 and 80 695 cm^{-1} for $(1)1_u$ $(5s[3/2]_2)$ and $(1)O_u^+$ $(5s[3/2]_1)$ respectively, while the calculated vertical transitions (at $R=7.8\,a_0$) are 79 949 and 80 789 cm^{-1}. As concerns the $(2)O_u^+$ $(5s'[1/2]_1)$ state the minimum of which lies in the medium distance range ($R_e=6.94\,a_0$), the calculated well depth ($D_e=458\ \text{cm}^{-1}$) and ω_e constant (50 cm^{-1}) are in good agreement with the values given by Tanaka ($D_e=464\ \text{cm}^{-1}$, $\omega_e=43.3\ \text{cm}^{-1}$) and also with the values obtained in the calculation of Gadéa *et al.*[30] as shown in Table XIII. Further discussion about those states is carried on in the part dealing with fluorescence studies.

The present work also allows the examination of band systems related to the upper states, i.e., system IV (92 562–92 530 cm^{-1}), system V (93 069–93 022 cm^{-1}), system VI (93 436–93 414 cm^{-1}), and system VII (94 199–93 941 cm^{-1}). All systems concern species dissociating between $5p[5/2]_3$ and $5p[1/2]_0$. We first examine the O_u^+ potentials. In the diabatic representation [Fig. 6(b)], states $(IV)O_u^+$ $(5p[3/2]_2)$ and $(V)O_u^+$ $(5p[1/2]_0)$ are attractive and both cross the repulsive $(III)O_u^+$ $(5p[5/2]_2)$ state. The crossing between $(III)O_u^+$ and $(IV)O_u^+$ is located around $R=7\,a_0$, while the crossing between $(III)O_u^+$ and $(V)O_u^+$ occur around $R=6.25\,a_0$. Considering the adiabatic states [Fig. 6(a)], the avoidances result in a hump in $(3)O_u^+$ $(5p[5/2]_2)$, while $(4)O_u^+$ $(5p[3/2]_2)$ exhibits a well of 379 cm^{-1} at $R_e=7.26\,a_0$, and $(5)O_u^+$ $(5p[1/2]_0)$ has a well of 828 cm^{-1} at $R=6.08\,a_0$. Thus in the adiabatic representation, only states $(4)O_u^+$ and $(5)O_u^+$ are attractive and are likely to be the upper states of bound–bound transitions around the distance of interest. The calculated vertical transitions from the ground state are, respectively, 93 123 and 94 278 cm^{-1}. In the 1_u manifold [Figs. 8(a) and 8(b)], there is only one diabatic attractive state, namely $(VII)1_u(5p[3/2]_1)$. However, this state crosses the repulsive states $(V)1_u(5p[5/2]_3)$ and $(VI)1_u(5p[5/2]_2)$. This crossing results in rather complex shapes for the adiabatic states. State $(5)1_u(5p[5/2]_3)$ presents a hump around $R=7.5\,a_0$ and becomes attractive at shorter distance, $(6)1_u(5p[5/2]_2)$ has a quasibound minimum located 173 cm^{-1} above the asymptote and $(7)1_u(5p[3/2]_1)$ exhibits a shallow well of 88 cm^{-1} at $R=7.48\,a_0$. Vertical transitions

TABLE VIII. Spectroscopic constants of 3_u states.

State	Dissociation	Minima	$R_e(a_0)$	$D_e(\text{cm}^{-1})$	$\omega_e(\text{cm}^{-1})$
Adiabatic					
1	$5p[5/2]_3$	1	5.16	223	190
		2	6.76	732	49
2		1	5.65	6000	353
Diabatic					
I	$5p[5/2]_3$	1	6.78	709	46
II		1	5.16	6968	177

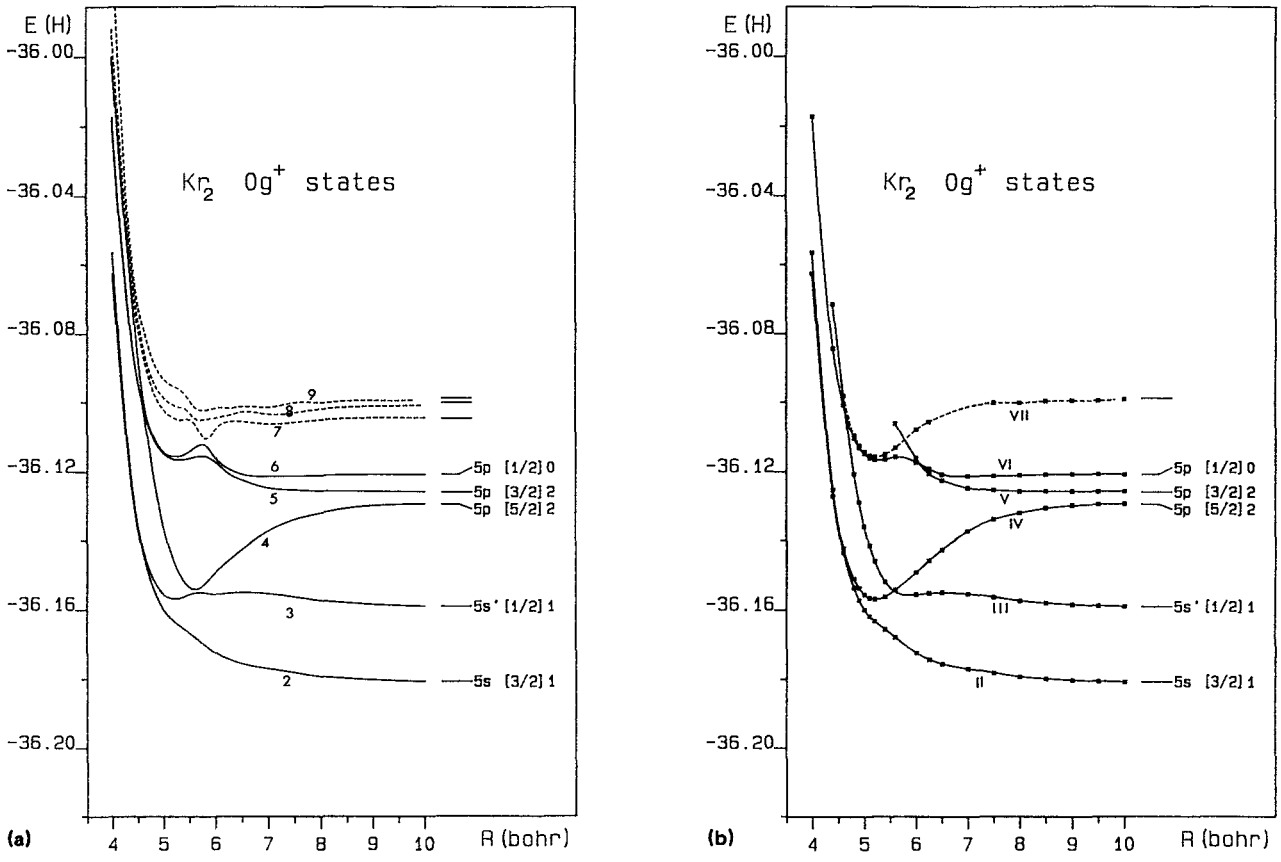

FIG. 11. Potential energy curves of the excited O_g^+ states of Kr_2^*. (a) adiabatic states; (b) diabatic states (the squares indicate the calculated potential values which were conserved for drawing the diabatic potentials). The dashed lines refer to potentials dissociating adiabatically higher than Kr*(5*p*).

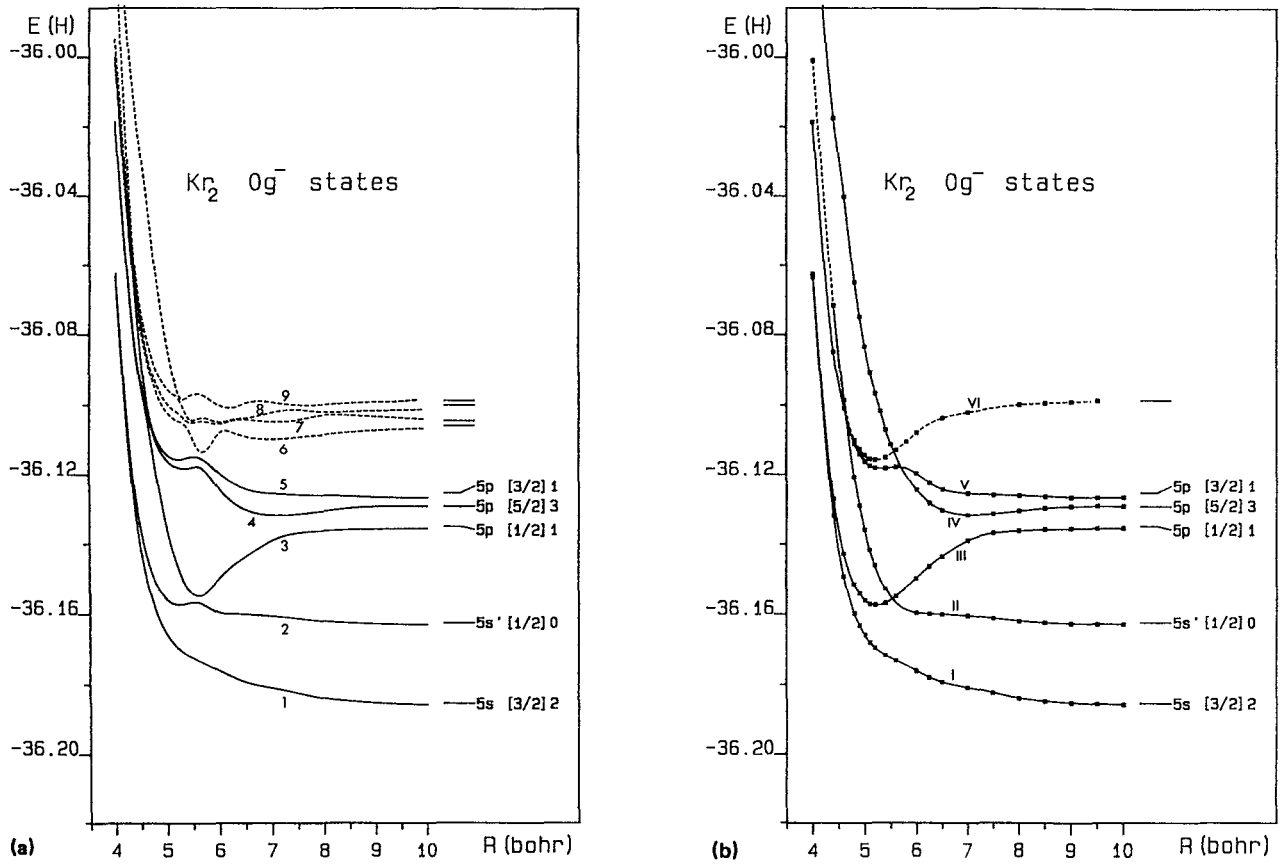

FIG. 12. Potential energy curves of the excited O_g^- states of Kr_2^*. (a) adiabatic states; (b) diabatic states (the squares indicate the calculated potential values which were conserved for drawing the diabatic potentials). The dashed lines refer to potentials dissociating adiabatically higher than Kr*(5*p*).

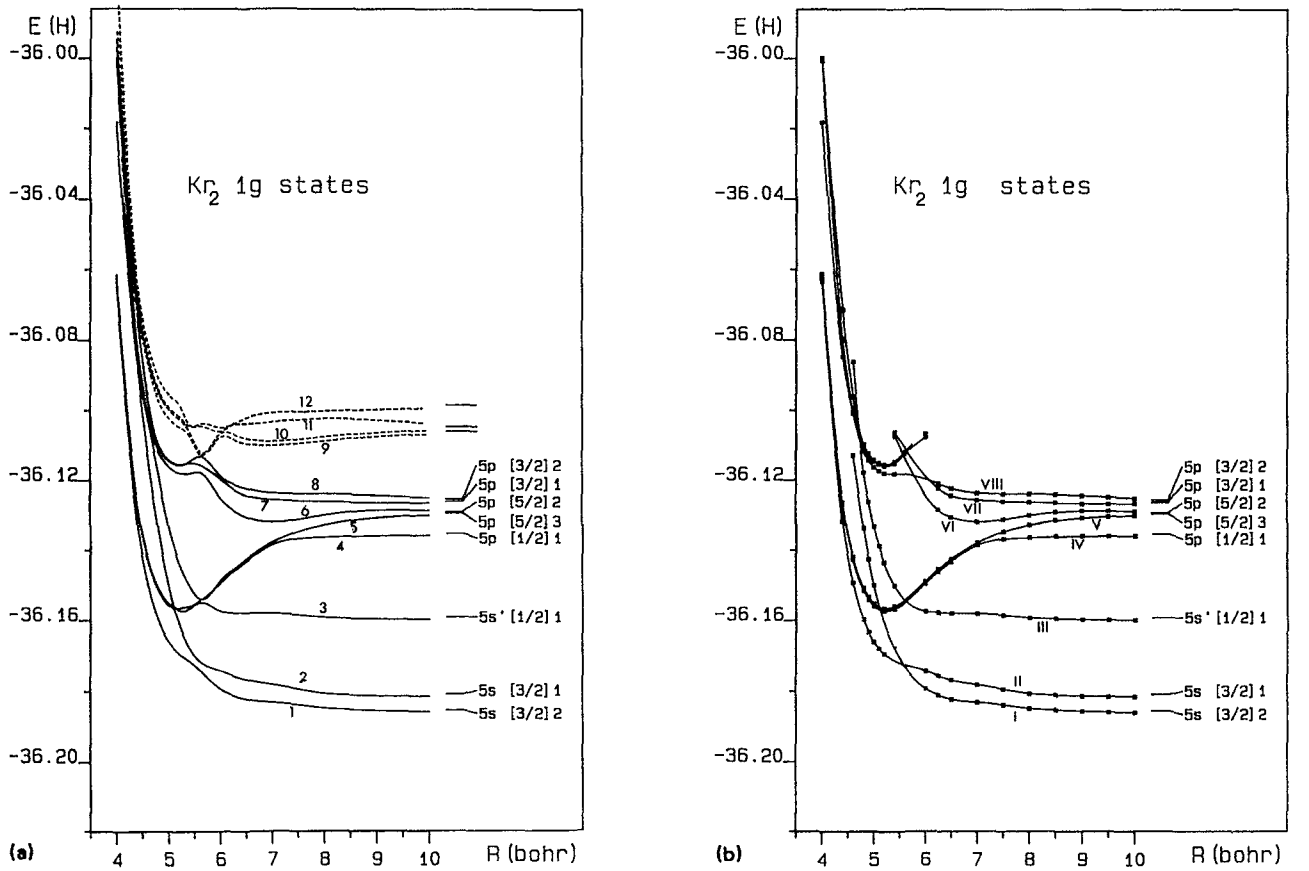

FIG. 13. Potential energy curves of the excited 1_g states of Kr_2^*. (a) adiabatic states; (b) diabatic states (the squares indicate the calculated potential values which were conserved for drawing the diabatic potentials). The dashed lines refer to potentials dissociating adiabatically higher than Kr*(5*p*).

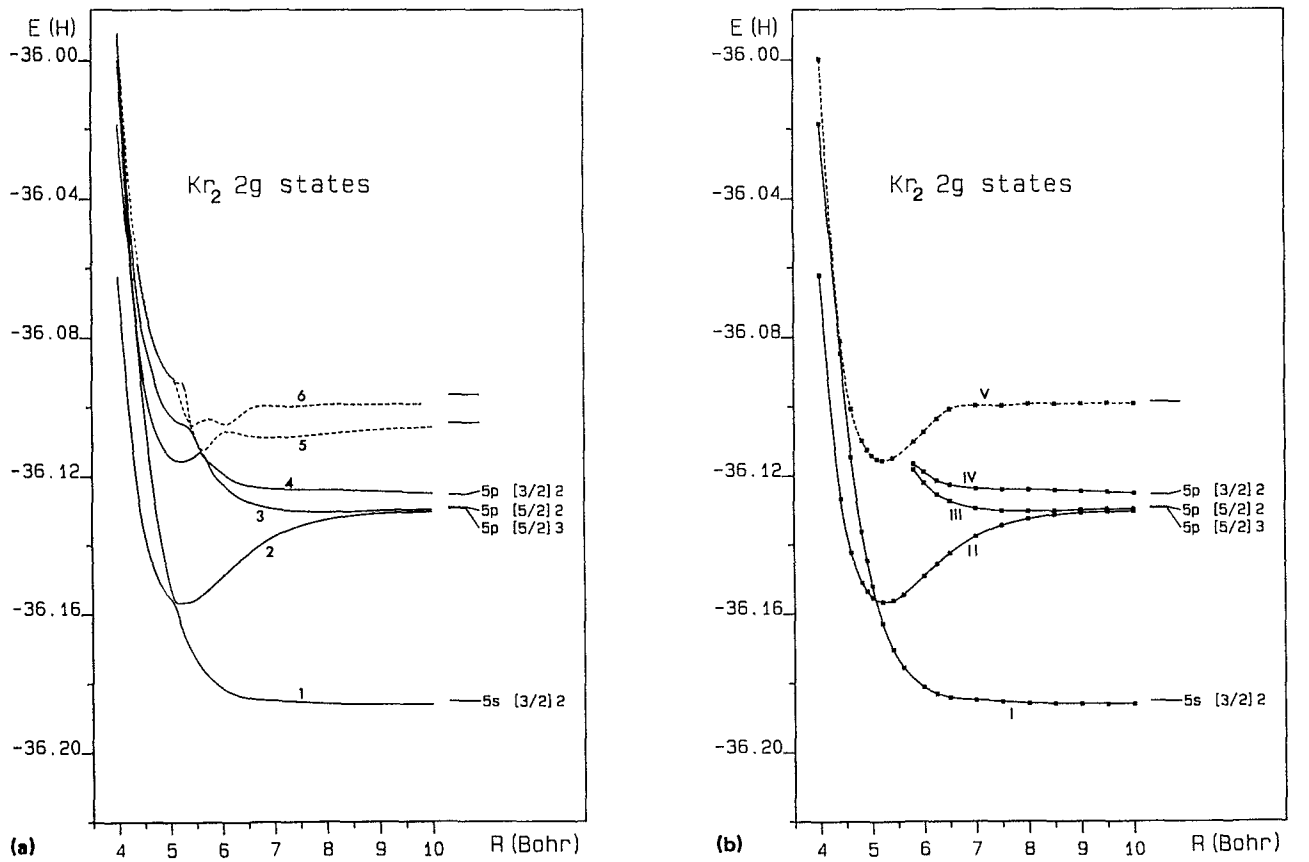

FIG. 14. Potential energy curves of the excited 2_g states of Kr_2^*. (a) adiabatic states; (b) diabatic states (the squares indicate the calculated potential values which were conserved for drawing the diabatic potentials). The dashed lines refer to potentials dissociating adiabatically higher than Kr*(5*p*).

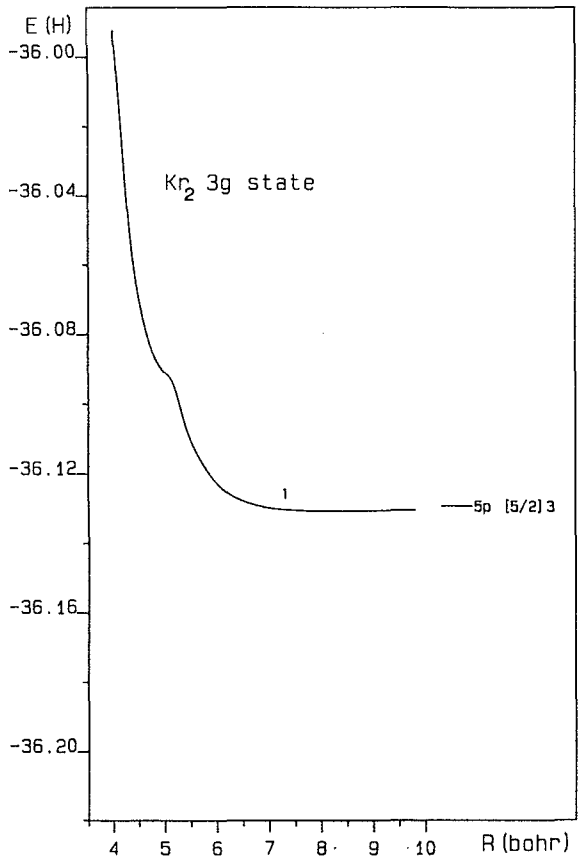

FIG. 15. Potential energy curves of the excited 3_g states of Kr_2^* (adiabatic state).

from the ground state towards states $(5)1_u$, $(6)1_u$, and $(7)1_u$ are 92 625, 92 906, and 93 244 cm^{-1}, respectively. If we compare the calculated transitions with Tanaka's results, it seems that system VII can be unambiguously assigned to state $(5)O_u^+(5p[1/2]_0)$, confirming Tanaka's proposal. The situation is less clear for the other band systems. States $(4)O_u^+(5p[3/2]_2)$ and $(7)1_u(5p[3/2]_1)$ are likely to correspond to band systems (V) and (VI). However, the two transitions in the calculation are less separated than the observed bands and the transition towards state $(6)1_u$ is also rather close. As concerns system (IV), the closest transition corresponds to state $(5)1_u$, which indeed presents a hump as presumed by Tanaka who mentioned an overlap with a weak absorption continuum. One should, however, be aware that the straight application of the Franck–Condon principle (vertical transitions towards adiabatic states) within the framework of the Born–Oppenheimer approximation is certainly questionable in the present situation, since the different curves are far from being well separated in the distance range concerned with the transitions.

2. Gerade states

We now turn to two photon spectra which concern g states also dissociating between $5p[3/2]_3$ and $5p[1/2]_0$. Dehmer and Pratt[55] report one band system with a vibrational progression (94 024–93 838 cm^{-1}) and another system with two terms (93 153, 93 142 cm^{-1}). Echt and coworkers[54] have also observed two band systems, one with a rather long vibrational progression (92 301–91 772 cm^{-1}), the second with a short progression (92 268–92 192 cm^{-1}). Three adiabatic O_g^+ states, namely $(4)O_g^+$, $(5)O_g^+$, $(6)O_g^+$, four 1_g states, namely $(5)1_g$, $(6)1_g$, $(7)1_g$, $(8)1_g$, and two 2_g states, namely $(2)2_g$ and $(3)2_g$ are connected with the $5p$ asymptotes of interest. As shown in Table IX, state $(4)O_g^+(5p[5/2]_2)$ is strongly bound, state $(5)O_g^+(5p[3/2]_2)$ has a very shallow well above the asymptote at $R = 8.16\ a_0$, while $(6)O_g^+(5p)[1/2]_0)$ is bound by 152 cm^{-1} at $R = 6.82\ a_0$. Vertical transitions from the

TABLE IX. Spectroscopic constants of O_g^+ states. Negative dissociation energies refer to minima above the asymptote.

State	Dissociation	Minima	$R_e(a_0)$	$D_e(cm^{-1})$	$\omega_e(cm^{-1})$
Adiabatic					
1	$4p^6(^1S_0)$	1	7.84	250	23
2	$5s[3/2]_1$	Repulsive			
3	$5s'[1/2]_1$	1	5.21	−441	184
4	$5p[5/2]_2$	1	5.61	5442	261
5	$5p[3/2]_2$	1	5.28	−2016	151
6	$5p[1/2]_0$	1	5.22	−1088	145
		2	6.82	152	63
Diabatic					
I	$4p^6(^1S_0)$	1	7.84	250	23
II	$5s[3/2]_1$	Repulsive			
III	$5s'[1/2]_1$	1	5.84	−686	115
IV	$5p[5/2]_2$	1	5.22	6039	171
V	$5p[3/2]_2$	Repulsive			
VI	$5p[1/2]_0$	1	5.29	−871	145
		2	6.82	149	69
VII		1	5.22	2454	176

TABLE X. Spectroscopic constants of O_g^- states. Negative dissociation energies refer to minima above the asymptote.

State	Dissociation	Minima	$R_e(a_0)$	$D_e(cm^{-1})$	$\omega_e(cm^{-1})$
Adiabatic					
1	$5s[3/2]_2$	Repulsive			
2	$5s'[1/2]_0$	1	5.21	−1099	196
3	$5p[1/2]_1$	1	5.59	4363	257
4	$5p[5/2]_3$	1	5.32	−2360	152
		2	7.07	580	63
5	$5p[3/2]_1$	1	5.20	−2080	210
Diabatic					
I	$5s[3/2]_2$	Repulsive			
II	$5s'[1/2]_0$	Repulsive			
III	$5p[1/2]_1$	1	5.23	4910	165
IV	$5p[5/2]_3$	1	7.07	580	64
V	$5p[3/2]_1$	1	5.31	−1552	130
VI		1	5.22	3792	170

ground state towards these three O_g^+ states are, respectively, 91 860, 93 352, and 94 357 cm^{-1}. The situation is more complex in the 1_g manifold, since there is obviously a multiple avoided crossing in the region $7\,a_0 < R < 8\,a_0$ involving states $(4)1_g$, $(5)1_g$, and $(6)1_g$. As a result, state $(5)1_g$ [and also $(4)1_g$ not under concern here] are strongly bound; state $(6)1_g$ is bound by 635 cm^{-1} at $R = 6.99\,a_0$. State $(7)1_g$ is repulsive in the considered area while state $(8)1_g$ has a very shallow well located 330 cm^{-1} above the asymptote. The transition towards $(5)1_g$, $(6)1_g$, and $(8)1_g$ are 91 678, 92 320, and 93 765 cm^{-1}. Finally, state $(2)2_g$ is again very strongly bound, while state $(3)2_g$ has a well of 307 cm^{-1} at $R = 7.98\,a_0$. The corresponding transitions are 91 722 and 92 331 cm^{-1}. The bluest band observed by Dehmer and Pratt[55] can be attributed to the $(6)O_g^+$ $(5p[1/2]_0)$ state. The experimental vibrational spacings indeed range between 52 and 40 cm^{-1}, which is compatible with excited vibrational levels of the $(6)O_g^+$ state with a minimum at $R = 6.82\,a_0$ and an ω_e value of 63 cm^{-1}. From an energetic point of view, $(8)1_g$ could also be a proper candidate, however, this state is not absolutely bound, and moreover the calculated ω_e is only 31 cm^{-1}. The calculated transition closest to the second band observed by Dehmer and Pratt corresponds to the $(5)O_g^+$ state. However, this state is only relatively bound in our calculation while the wavelengths given by Dehmer and Pratt correspond to a well of 109 cm^{-1} for the upper

TABLE XI. Spectroscopic constants of 1_g states. Negative dissociation energies refer to minima above the asymptote. Values with a star (*) correspond to minima on the adiabatic curves which are very close to an avoided crossing and may have poor physical meaning.

State	Dissociation	Minima	$R_e(a_0)$	$D_e(cm^{-1})$	$\omega_e(cm^{-1})$
Adiabatic					
1	$5s[3/2]_2$	Repulsive			
2	$5s[3/2]_1$	Repulsive			
3	$5s'[1/2]_1$	1	5.26	−332	260
4	$5p[1/2]_1$	1	5.16	4736	396.0(*)
5	$5p[5/2]_3$	1	5.64	5400	299
6	$5p[5/2]_2$	1	5.31	−2358	155
		2	6.99	635	73
7	$5p[3/2]_1$	1	5.20	−2226	225
8	$5p[3/2]_2$	1	5.22	−2177	165
		2	7.40	−331	31.0
Diabatic					
I	$5s[3/2]_2$	Repulsive			
II	$5s[3/2]_1$	Repulsive			
III	$5s'[1/2]_1$	Repulsive			
IV	$5p[1/2]_1$	1	5.21	4874	156
V	$5p[5/2]_3$	1	5.21	5954	160
VI	$5p[5/2]_2$	1	6.97	636	71
VII	$5p[3/2]_1$	Repulsive			
VIII	$5p[3/2]_2$	1	7.42	−331	30

TABLE XII. Spectroscopic constants of 2_g states. Negative dissociation energies refer to minima above the asymptote.

State	Dissociation	Minima	$R_e(a_0)$	$D_e(\text{cm}^{-1})$	$\omega_e(\text{cm}^{-1})$
Adiabatic					
1	$5s[3/2]_2$	Repulsive			
2	$5p[5/2]_3$	1	5.15	6027	358
3	$5p[5/2]_2$	1	5.22	− 2917	195
		2	7.98	307	36
4	$5p[3/2]_2$	Repulsive			
Diabatic					
I	$5s[3/2]_2$	Repulsive			
II	$5p[5/2]_3$	1	5.24	6001	127
III	$5p[5/2]_2$	1	7.99	299	37
IV	$5p[3/2]_2$	Repulsive			
V		1	5.22	3753	173

state. One should nevertheless notice that the minimum of $(5)O_g^+$ is situated above the ground state minimum, which could explain the strong (0,0) term observed experimentally. Moreover, the absence of vibrational progression is compatible with a very shallow well. A 100–150 cm^{-1} underestimation of the bound character of this state in our calculation could explain the discrepancy with experiment.

The band of Echt *et al.*[54] with a short vibrational progression is correlated by the authors with the $5p[5/2]_2$ asymptote. Two states are in competition around 92 200 cm^{-1}, namely $(6)1_g$ and $(3)2_g$, which have a minimum at large distance, respectively, at 6.99 and 7.98 a_0. Because of the very strong (0,0) transition reported by Echt *et al.*, the choice of $(3)2_g$ is to be preferred since the Franck–Condon factors are more favorable. Moreover, the calculated well characteristics of $(3)2_g$ ($D_e = 307\ \text{cm}^{-1}$, $\omega_e = 36\ \text{cm}^{-1}$) are closer to the proposals of Echt *et al.* ($D_e = 220\ \text{cm}^{-1}$, $\Delta G_{1/2} = 27.6\ \text{cm}^{-1}$) than the characteristics of $(6)1_g$ ($D_e = 635\ \text{cm}^{-1}$, $\omega_e = 73\ \text{cm}^{-1}$). The situation is *a priori* less clear for the band system related to the long vibrational progression, since at least three states remain as possible candidates, namely $(4)O_g^+$ $(5p[5/2]_2)$, $(6)1_g(5p[5/2]_2)$, and $(2)2_g(5p[5/2]_3)$. However, the close embedding of the two band systems observed by Echt *et al.* gives a preference for state $(6)1_g$, which as already mentioned, is almost degenerate at $R = 7.84\,a_0$ with state $(3)2_g$ previously assigned to the short progression. The ω_e value of 73 cm^{-1} is in good agreement with the first experimental spacing $\Delta G'_{1/2} = 75.4$ cm^{-1}. Although the observed levels of Echt *et al.* lie below the $5p[5/2]_2$ asymptote, the extrapolation of their results leads the authors to correlate this long progression to the $5p[3/2]_2$ asymptote and propose a well depth $\geqslant 1480\ \text{cm}^{-1}$. Correlation with the $5p[5/2]_2$ level would yield a well depth $\geqslant 636\ \text{cm}^{-1}$, which is very close to the calculated depth of the $(6)1_g$ state ($D_e = 635\ \text{cm}^{-1}$) obviously adiabatically correlated with $5p[5/2]_2$. Interestingly enough, one may notice that state $(6)1_g$ has a hump of $\sim 100\ \text{cm}^{-1}$ above the asymptote around 9 bohr, as a result of a long distance avoided crossing, which gives consistency to diabatic extrapolation towards a higher asymptote. Beyond the comparison with the existing experimental data of Echt *et al.* and Dehmer *et al.*, the present calculation predicts two photon transitions from the ground state at wave numbers shorter than 92 200 cm^{-1} implying state $(4)O_g^+$, $(4)1_g$, $(5)1_g$, and $(2)2_g$, provided that the transition probabilities are nonvanishing.

B. Fluorescence from the lowest excimer states

Emission spectra concern vibrational levels of states $(1)1_u(5s[3/2]_2)$, $(1)O_u^+(5s[3/2]_1)$, and $(2)O_u^+(5s'[1/2]_1)$. One can distinguish fluorescence spectra according to the distance range associated with the upper state. Emission from the low vibrational levels yield either continua (when the repulsive part of the ground state is reached) or discrete spectra (when the ground state van der Waals region is involved). As mentioned in Sec. IV B, a large uncertainty remains as concerns the repulsive part of the ground state, resulting in significant differences for the calculation of transition energies. We use in the following, the present theoretical determination of the ground state correction and apply the same correction of 2500 cm^{-1} for the asymptotic transitions.

1. Excimer emission maximum

The second continuum of krypton corresponds to a bound–free transition between the relaxed vibrational levels and the ground state. The first analysis was performed by Tanaka *et al.*[37] They reported a fluorescence maximum around 66 640 cm^{-1} (150 nm). Vuv emission is due to both $(1)1_u$ $(5s[3/2]_2)$ and $(1)O_u^+$ $(5s[3/2]_1)$. However, the radiative lifetime of $(1)1_u$ relaxed levels is almost 100 times larger than the lifetime of $(1)O_u^+$.[57] The time dependence of fluorescence is therefore characterized by a slow and a fast component. Time resolved techniques allow separation of the two components of the emission. Recently, Morikawa *et al.*[44] estimated two maxima of emission at low density, around 69 100 and 69 850 cm^{-1} for $(1)1_u$ and $(1)O_u^+$ states, respectively. These experimental results are likely to

TABLE XIII. Spectroscopic constants of Kr_2 excimer states dissociating into $Kr^*(5s,5s')$. (*): values deduced from experimental molecular ionization limit from the $(1)1u$ state and the experimental dissociation energy of the $1(1/2)u$ state of Ng *et al.* (Ref. 61).

State	$R_e(a_0)$	$D_e(cm^{-1})$	$D_0(cm^{-1})$	$\omega_e(cm^{-1})$	Authors
$(1)1u$					
				166	Zamir *et al.*[a]
	5.21	3866	3780	172	Gadéa *et al.*[b]
			4823(*)		Sauerbrey *et al.*[c]
	4.18	5807	5685	244.5	LaRocque *et al.*[d]
		4851(*)	4764(*)	172	Killeen and Eden[e]
		4937(*)	4841(*)	195,189	Ediger and Eden[f]
	5.02	5600	5517	166.3	Barzen *et al.*[g]
	5.24	3928	3847	163	This work
$(1)O_u^+$					
	5.21	4070	3978	184	Gadéa *et al.*[b]
	4.58	5629	5519	219.5	LaRocque *et al.*[d]
	5.02	5600	5517	166.3	Barzen *et al.*[g]
	5.22	4137	4051	173	This work
$(2)O_u^+$					
		464	442.8	43.3	Tanaka *et al.*[h]
	7.14	454	434	41	Gadéa *et al.*[b]
	6.99	465	443	43.8	LaRocque *et al.*[d]
	6.94	458	433	50	This work

[a] Reference 47.
[b] Reference 30.
[c] Reference 50.
[d] Reference 42.
[e] Reference 51.
[f] Reference 52.
[g] Reference 43.
[h] Reference 37.

correspond to emissions from the bottom of the wells of the two states ($v' = 0$ levels). At $R = 5.2\ a_0$, which is the equilibrium distance of the two states, the vertical transitions towards the ground state are found to be 69 469 and 70 259 cm^{-1}, showing a $\sim 400\ cm^{-1}$ discrepancy with the experimental estimations.

2. Energy separation between $(1)1_u$ and $(1)O_u^+$

The experiment of Morikawa *et al*[44] measures the energy separation between $(1)1_u$ and $(1)O_u^+$ over a wide density range. The averaged value was found to be 484 cm^{-1} (60 meV). Analyzing solid krypton luminescence, Dössel *et al.*[72] proposed a value of 887 cm^{-1} (110 meV). The distance between the two potential curves in the present work is 790 cm^{-1}, in close agreement with the previous calculation of Gadéa *et al.*[31] (740 cm^{-1}) while the atomic separation is 944 cm^{-1}.[65] All those results converge to indicate that the $(1)O_u^+$ well is deeper than the $(1)1_u$ well, in disagreement with the estimations of Larocque *et al.*[42] (see Table XIII) and the assumption made by Barzen *et al.*[43]

3. Left turning point of $(1)O_u^+$

Möller *et al.*[41] have measured the transition energy from the left turning point (LTP) of $(1)O_u^+$ towards the ground state to be 55 230 cm^{-1} (181 nm). Relying on the unpublished result of Foreman *et al.*[71] for the ground state repulsive shape, they estimated the LTP internuclear distance to be $r_{LTP} = 4.29\ a_0$. The present calculation yields $r_{LTP} = 4.53\ a_0$ and the corresponding transition is found to be 58 593 cm^{-1}, showing a $\sim 3400\ cm^{-1}$ difference with the experimental transition. If we consider that our potential for the ground state is more repulsive than the expression of Foreman *et al.* it is likely that our calculated r_{LTP} is too large. Because of the very fast variation of the ground state in this area, the transition energy also varies very quickly with r_{LTP}. A reduction of the theoretical value by a $0.1\ a_0$ for instance would yield a transition of 54 424 cm^{-1}, lower than the experimental value.

4. Fluorescence features in the large distance range

Larocque *et al.*[42] studied induced fluorescence through selective excitation (vuv laser) of dimers formed in supersonic beam expansions. They could therefore probe the unrelaxed highly vibrational levels ($v'' = 30$–40) of states $(1)1_u$ and $(1)O_u^+$. They also reported emission measurements concerning the bound vibrational states of $(2)O_u^+$ which were already extensively studied in absorption experiments and mentioned in Sec. V A 1. The reported spectroscopic data for this state ($D_e = 465\ cm^{-1}$, $\omega_e = 43.8\ cm^{-1}$) are in excellent agreement with other experimental or theoretical determinations (Table XIII) and with the present calculated results. As concerns the lowest electronic states $(1)1_u$ and $(1)O_u^+$, the spectroscopic constants of Larocque *et al.* are extrapolated from the data obtained for the unrelaxed levels, and are therefore subject to the validity of the extrapolation process. Their well depths and ω_e constants are substantially larger than other experimental or theoretical values quoted in Table XIII. As already alluded to in Sec. V B 2, the $(1)1_u$–$(1)O_u^+$ separation (1123 cm^{-1}) thus obtained is larger than the values of other authors and corre-

sponds to a larger stabilization of the lowest state. The potential curves proposed in Ref. 42 are rather unlikely and seem to be double valued in the inner part whereas both curves cross each other twice in the outer part.

C. Transient absorption

Transient absorption reported in the literature concerns states of gerade symmetry populated from the relaxed levels of $(1)O_u^-(5s[3/2]_2)$, $(1)1_u(5s[3/2]_2)$ and $(1)O_u^+(5s[3/2]_1)$. From theory, only states $(1)O_u^+$ and $(1)1_u$ have nonzero transition dipole moments with the ground state and thus a finite lifetime. Fluorescence of the $(1)O_u^-$ state towards the ground state is forbidden. However, in actual transient absorption experiments $(1)1_u$ and $(1)O_u^-$, which are almost degenerate (a separation of 12 cm^{-1} at $R = 5.2\ a_0$) are easily collisionally mixed. The excimer lifetime is therefore increased from 178 ns for the pure $(1)1_u$ state to 265 ns[57] for the mixture experimentally observed. The long lifetime of the 1_u, O_u^- mixture, in contrast with the short lifetime[44] of the $(1)O_u^+$ (3.4 ns), explains that most experiments are concerned with absorption from $(1)1_u$, O_u^-. The symmetry allowed one-photon transitions are $1_u \rightarrow O_g^+$, O_g^-, 1_g, 2_g, and $O_u^- \rightarrow O_g^-$, 1_g. In the following, the discussion is structured according to the energy range of the absorption spectra.

1. Infrared absorption in the 7200–8700 cm^{-1} energy range

Wide absorption bands were observed by Arai *et al.*[46] around 7700 cm^{-1} (1300 nm) and Kasama *et al.*[48] between 7260 cm^{-1} (0.90 eV) and 8630 cm^{-1} (1.07 eV). This energy range concerns the lowest g states adiabatically correlated with asymptotes $5s[3/2]_1$ and $5s[3/2]_2$. Although they resemble some features of the underlying $(3)\Sigma_g^+$ and $(1)\Sigma_g^+\{\Lambda S\Sigma\}$ parents which present a quasibound well,[29] the gerade Ω states $(2)O_g^+$, $(1)O_g^-$, $(1)1_g$, are all essentially repulsive with some inflections due to the particular shapes of the $^{3,1}\Sigma_g^+$ parents (see above) or intraconfigurational avoided crossings. This repulsive character is in contradiction with the estimations of Barr,[4] based on Mulliken's analysis, which seem to overestimate the bound character of the parent states. Our calculation indicates that only bound–free transitions are likely to occur, which is consistent with the broad character of the observed bands, and is confirmed by a recent kinetic analysis.[57] The calculated vertical transitions at $R = 5.2\ a_0$ from $(1)1_u$ towards $(1)O_g^-$, $(1)1_g$, and $(2)O_g^+$ are 7362, 7390, and 8719 cm^{-1}, respectively, those from $(1)O_u^-$ towards $(1)O_u^-$ and $(1)1_g$ being almost identical to the previous ones. These values are fairly consistent with the experimental results.

2. Near infrared absorption around 10 000 cm^{-1}

The same authors[46] also report four absorption lines around 10 000 cm^{-1}, respectively, at 10 112, 10 167, 10 261, and 10 354 cm^{-1}. There are five adiabatic states in this energy range, namely $(3)O_g^+(5s'[1/2]_1)$, $(2)O_g^-(5s'[1/2]_0)$, $(3)1_g(5s'[1/2]_1)$, $(4)1_g(5p[1/2]_1)$, and $(2)2_g(5p[5/2]_3)$. All five states result from the characteristic situation of strongly bound upper diabatic state $(IV)O_g^+$, $(III)O_g^-$, $(IV)1_g$, $(V)1_g$, and $(II)2_g$ correlated with the $5p$ configuration and predissociated by repulsive states $(III)O_g^+$, $(II)O_g^-$, $(II)1_g$, $(III)1_g$, and $(I)2_g$ correlated with the $5s'$ configuration. In this particular case, the diabatic picture is probably more adequate, because of the small interaction. Our transitions from $(1)1_u$ towards the five diabatic states at $R = 5.2\ a_0$ are 10 021, 10 054, 10 135, 10 196, and 10 217 cm^{-1}, the allowed transitions from $(1)O_u^-$ to the same states being again almost identical. Although the knowledge of transition moments is compulsory in order to provide a one to one assignment, these calculated transitions are in good correspondence with the observed terms. The maximum splitting of the five states is found to be 194 cm^{-1}, also in agreement with the observed maximal separation 242 cm^{-1}.

3. Transition to higher molecular Rydberg species

Transitions from $(1)1_u$, O_u^- were also experimentally observed towards higher excited states. First, Zamir[47] reported a group of five lines obtained at higher pressure (and probably affected by a redshift) in the visible range at 19 915, 18 720, 18 550, 18 410, and 17 660 cm^{-1} (502, 534, 539, 543, and 566 nm). More recent experiments at lower pressure performed by the group of Eden[51,52] and Sauerbrey *et al.*[50] have probed the same energy range and groups of lines converging towards the ionization limit were attributed to Rydberg series. The authors generally invoke two different Rydberg series, using the $\{\Lambda S\Sigma\}$ representation, namely $5s\ ^3\Sigma_u^+ \rightarrow mp\ ^3\Sigma_g^+$ and $5s\ ^3\Sigma_u^+ \rightarrow np\ ^3\Pi_g$. With the present notation, the initial state is $(1)1_u, O_u^-$, while the final states are $\{\Omega\}$ states with $\{\Lambda S\Sigma\}$ parents characterized by $[^2\Sigma_u^+]\sigma_u mp$ or $[^2\Sigma_u^+]\pi_u np$ configurations, respectively.

Two papers, Refs. 51 and 52, explicitly classify their lines as belonging to both series. In the work of Killeen and Eden,[51] the observed lines at 18 805 cm^{-1} (531.64 nm) and 22707 cm^{-1} (440.26 nm) were assigned as the $m = 6$ and 7 terms of the $mp\ ^3\Pi_g$ series ($\Delta v = 0$), whereas observed lines at 12 140 cm^{-1} (823.40 nm) and 20 017 cm^{-1} (499.42 nm) were assigned as the $n = 6$ and 7 terms of the $np\ ^3\Sigma_g^+$ series ($\Delta v = 0$). Later, Ediger and Eden[52] reported lines at 22 722 cm^{-1} (439.97 nm) and 20 025 cm^{-1} (499.23 nm), which were, respectively, identified as the $7p\ ^3\Pi_g$ and $7p\ ^3\Sigma_g^+$ terms

First, it seems that the quantum number attribution of the second series is very unlikely since it yields dissociation energies which are systematically larger than the Kr_2^+ ion dissociation energy (by a factor 2 for the first term of the series, i.e., $D_e = 1.952$–2.011 eV) in Ref. 51. A more likely attribution would consist in reducing this quantum number by one, as already recently suggested by the authors themselves[73] for the argon case also examined in the same paper.[51] This would yield the identification of the 12 140 cm^{-1} line as the $5p\ ^3\Sigma_g^+$ term, and the 20 017/20 025 cm^{-1} line as the $6p\ ^3\Sigma_g^+$ term and would mean that the $6p^3\Pi_g$ states (18 805 cm^{-1} line) lie below the $6p^3\Sigma_g^+$ states (20 017/20 025 cm^{-1} line) by 1200 cm^{-1}. This assignment is somewhat

contradictory to the assignment previously given by Sauerbrey *et al.*[50] who attribute a line at 20 040 cm^{-1} (499.0 nm) as the $m = 6$ term of the $mp\ ^3\Pi_g$ series, tentatively identifying the Ω components as 1_g or 2_g.

Our calculation provides eight $\{\Omega\}$ relevant states in the 18 000–20 000 cm^{-1} energy range. According to our diabatic scheme, they can be classified into two groups with rather different features, lying close together within a $\sim 600\ cm^{-1}$ range. States $(VI)O_g^-$, $(VII)O_g^+$, $(IX)1_g$, $(X)1_g$, and $(V)2_g$ have $^{3,1}\Pi_g$ parents with dominant configuration $[^2\Sigma_u^+]\pi_u 6p$ over the whole distance range. They are correlated with the $6p$ levels and are strongly bound with respect to this asymptote. The respective transition energies from $(1)1_u$ towards those states are 19 148, 19 163, 19 167, 19 186, and 19 246 cm^{-1}, respectively. The second group includes states $(V)O_g^-$, $(VI)O_g^+$, and $(VIII)1_g$ which have $^{3,1}\Sigma_g^+$ parents. Those states are characterized by type (ii) behavior (see Sec. III). They have $[^2\Sigma_u^+]\sigma_u 6p$ character at short distance which transforms slowly into $[^2\Sigma_g^+]\sigma_g 5p$ character at long distance, with a weak relative well followed by a barrier to dissociation. They are thus not fully diabatic. The transition energies towards states of the second group are 18 665, 18 667, and 18 784 cm^{-1}.

Thus we find that the $\{\Omega\}$ states related to $6p\ ^3\Pi_g$ lie above those related to $6p\ ^3\Sigma_g^+$. According to the present calculation, the upper state of the experimental transition at 18 805 cm^{-1} should be rather given a $6p\ ^3\Sigma_g^+$ assignment, whereas the line at 20 017/20 025 cm^{-1} is closer (however shifted) to the theoretical transition corresponding to Ω states related to $6p\ ^3\Pi_g$. One may notice that this theoretical ordering is in agreement with the recent high resolution analysis of Conrad *et al.*[68] for Ar_2^*, who cite similar findings for the Kr_2^* case.

It is likely that the interpretation given by the group of Eden should be revisited in the light of the present work and further experimental results at higher resolution be obtained.

4. Rydberg series limits

Fits of Rydberg series allowed Killeen and Eden, Ediger and Eden, and Sauerbrey *et al.* to derive the ionization limit from $(1)1_u, O_u^-$. Both series converge to the same limit. The values reported by Killeen and Eden[51] are 28 428.5 and 28 437 cm^{-1} while Ediger and Eden[52] propose 28 471.9 and 28 424 cm^{-1}. The series observed by Sauerbrey *et al.*[50] converges towards a limit of 28 490 cm^{-1}. The value obtained from the present calculation for Kr_2^* and Kr_2^+ is found to be 28 306 cm^{-1}, in excellent agreement with the experimental determinations. Thus despite of the probable underestimation of the dissociation energy for the Kr_2^+ ground state as well as for the $(1)1_u$, O_u^- and $(1)O_u^+$ states of Kr_2^*, the ionization energy is found to be very accurate, which indicates a systematic error in the $^2\Sigma_u^+$ core energy. The combination of the dissociation energy of Ng *et al.*[61] and Pratt and Dehmer[64] for Kr_2^+ (9279 cm^{-1}) and the ionization limits of the previous authors allows one to propose accurate estimates of the dissociation energy for $(1)1_u$, O_u^-, in the range 4850–4940 cm^{-1} (see values labeled by a star in Table XIII), smaller than the values proposed by Larocque *et al.*[42] or Barzen *et al.*,[43] while our calculated value is only 3850 cm^{-1}. Considering this $\sim 1000\ cm^{-1}$ error, and our calculation for the $(1)O_u^+$ state, one may estimate its actual dissociation energy to be in the range 5140–5230 cm^{-1}.

VI. CONCLUSION

We have presented in this work an extensive theoretical determination of the excited states dissociating into $Kr^*(5s,5s')$ and $Kr^*(5p)$, and some bound states correlated with higher atomic asymptotes, including *ab initio* calculation with spin–orbit pseudopotentials.

As concerns the lowest state of ungerade symmetry dissociating into $Kr^*(5s,5s')$, the present results do not differ significantly from previous calculations performed under similar conditions (same averaged relativistic pseudopotentials, MR perturbative CI), but using semiempirical spin–orbit coupling, as could be expected for these states. This is similar to the findings of Grein *et al.*[18,19] on Ne_2^* who compared Breit–Pauli-type calculations with the semiempirical procedure of Cohen and Schneider.

However, the use of pseudopotential spin–orbit coupling enables the determination of the fine structure in areas where the adiabatic excited states undergo strong configuration mixing in particular through avoided crossings.

A particular range of interest is the crossing between the gerade $\{\Omega\}$ states spanned by $^{3,1}\Pi_g$ $\{\Lambda S\Sigma\}$ parents dissociating into $Kr^*(5p)$ with the $\{\Omega\}$ states spanned by $^{3,1}\Pi_g$ and $^{3,1}\Sigma_g^+$ parents dissociating into $Kr^*(5s,5s')$. From a diabatic point of view, the upper states going to $Kr^*(5p)$ are strongly bound (by $\simeq 6000\ cm^{-1}$), whereas the potentials related to $Kr^*(5s)$ although showing inflections are purely repulsive, and the states related to $Kr^*(5s')$ exhibit a very shallow and flat minimum followed by a low barrier to dissociation. This result is very comparable to what was obtained in similar calculations of the gerade states of Ar_2^* also using spin–orbit pseudopotentials.[27] Our results show a satisfactory agreement with the infrared absorption results,[46,48] which supports the reliability of the present potential curves. The minima of the $5p$ bound states are very close to the $5s'[1/2]_1$ asymptotic level. The possibility of populating those minima after selective excitation of $5s'[1/2]_1$ levels certainly plays an important role for understanding the kinetics of excimer formation.[74] The crossing between $5p$ and $5s$, $5s'$ states is also crucial for interpreting interconfiguration excitation transfers in the krypton excimer.[56]

This work has also made possible the discussion of the absorption spectra from the ground state in particular the one-photon[37] and two-photon[54,55] experiments involving upper states related to the $5p$ asymptote around the equilibrium distance of the ground state. Finally, we were able to determine some higher states which correspond to the first members of Rydberg series observed in transient absorption from $(1)1_u$, O_u^-. The present theoretical results raise some questions about the assignments proposed by the group of Eden[51,52] whereas they seem to be in qualitative agreement

with the conclusions very recently proposed on Ar_2^* by Conrad *et al.*[68] The present work provides an overview of the electronic structure of the krypton dimer. Better insight into the interpretation of spectroscopic results should certainly be obtained through the knowledge of dipole transition moments between states involved in absorption or emission processes. Such work is in progress.

Note. Numerical values of the energies for the potential curves are available upon request (BITNET address: SPIEGEL @ FRPQT 51).

[1] R. S. Mulliken, Phys. Rev. **136**, A962 (1964).
[2] R. S. Mulliken, J. Chem. Phys. **52**, 5170 (1970).
[3] R. S. Mulliken, Radiat. Res. **59**, 357 (1974).
[4] T. L. Barr, D. Dee, and F. R. Gilmore, J. Quantum Spectrosc. Radiat. Transfer **15**, 625 (1975).
[5] D. C. Lorents, Physica C **82**, 19 (1976).
[6] R. S. Chang and D. W. Setser, J. Chem. Phys. **69**, 3885 (1978).
[7] J. S. Cohen and B. R. Schneider, J. Chem. Phys. **161**, 3230 (1974).
[8] B. R. Schneider and J. S. Cohen, J. Chem. Phys. **61**, 3240 (1974).
[9] W. R. Wadt, J. Chem. Phys. **68**, 402 (1978).
[10] W. R. Wadt, J. Chem. Phys. **73**, 3915 (1980).
[11] W. R. Wadt, P. J. Hay, and L. R. Kahn, J. Chem. Phys. **68**, 1752 (1978).
[12] W. C. Ermler, Y. S. Lee, K. S. Pitzer, and N. W. Winter, J. Chem. Phys. **69**, 976 (1978).
[13] P. A. Christiansen, K. S. Pitzer, Y. S. Lee, J. H. Yates, and W. C. Ermler, J. Chem. Phys. **75**, 5410 (1981).
[14] H. H. Michels, R. H. Hobbs, and L. A. Wright, J. Chem. Phys. **69**, 5151 (1978).
[15] S. Guberman and W. A. Goddard III, Phys. Rev. A **12**, 1203 (1975).
[16] S. Iwata, Chem. Phys. **37**, 251 (1979).
[17] F. Grein and S. D. Peyerimhoff, and R. J. Buenker, J. Chem. Phys. **82**, 353 (1985).
[18] F. Grein and S. D. Peyerimhoff, J. Chem. Phys. **87**, 4684 (1987).
[19] F. Grein, S. D. Peyerimhoff, and R. Klotz, Theoret. Chim. Acta **75**, (1987).
[20] R. P. Saxon and B. Liu, J. Chem. Phys. **64**, 3291 (1976).
[21] Ph. Durand and J.C. Barthelat, Theor. Chim. Acta **38**, 283 (1975).
[22] Y. Bouteiller, C. Mijoule, M. Nizam, J. C. Barthelat, J. P. Daudey, M. Pélissier, and B. Silvi, Mol. Phys. **65**, 295 (1988).
[23] C. Teichteil, M. Pélissier, and F. Spiegelmann, Chem. Phys. **81**, 273 (1983).
[24] P. A. Christiansen, Y. S. Lee, and K. S. Pitzer, J. Chem. Phys. **71**, 4445 (1979); P. A. Christiansen and P. S. Pitzer, *ibid.* **73**, 5160 (1980).
[25] F. Spiegelmann and J. P. Malrieu, Chem. Phys. Lett. **57**, 214 (1978).
[26] M. C. Castex, M. Morlais, F. Spiegelmann, and J. P. Malrieu, J. Chem. Phys. **75**, 5006 (1981).
[27] C. Teichteil and F. Spiegelmann, Chem. Phys. **81**, 283 (1983).
[28] J. H. Yates, W. Ermler, N. W. Winter, P. A. Christiansen, Y. S. Lee, and K. S. Pitzer, J. Chem. Phys. **79**, 6145 (1983).
[29] F. Spiegelmann and F. X. Gadéa, J. Phys. (Paris) **45**, 1003 (1984).
[30] F. X. Gadéa, F. Spiegelmann, M. C. Castex, and M. Morlais, J. Chem. Phys. **78**, 7270 (1983).
[31] M. Berman and U. Kaldor, Chem. Phys. **43**, 375 (1979).
[32] O. Vallée, N. Tran Minh, and J. Chapelle, J. Chem. Phys. **73**, 2784 (1980).
[33] Y. Mizukam and H. Nakatsuji, J. Chem. Phys. **92**, 6084 (1990).
[34] M. Krauss and W. J. Stevens, Annu. Rev. Phys. Chem. **35**, 357 (1984).
[35] J. C. Barthelat, M. Pélissier, and Ph. Durand, Phys. Rev. A **21**, 1773 (1981).
[36] K. Balasubramanian, Chem. Rev. **90**, 93 (1990).
[37] Y. Tanaka, K. Yoshino, and D. E. Freeman, J. Chem. Phys. **59**, 5160 (1973); Y. Tanaka, J. Opt. Soc. Am. **45**, 710 (1955).
[38] J. D. Gerardo and A. W. Johnson, Phys. Rev. A **10**, 1204 (1974).
[39] P. Laporte and H. Damany, J. Phys. (Paris) **40**, 9 (1979).
[40] Y. Matsuura and K. Fukuda, J. Phys. Soc. **50**, 933 (1981).
[41] T. Möller, J. Stapelfeldt, M. Beland, and G. Zimmerer, Chem. Phys. Lett. **117**, 301 (1985).
[42] P. E. Larocque, R. H. Lipson, P. R. Herman, and B. P. Stoicheff, J. Chem. Phys. **84**, 6627 (1986).
[43] K. Barzen, P. Wollenweber, and H. Schmoranzer, Chem. Phys. Lett. **142**, 79 (1987).
[44] E. Morikawa, R. Reininger, P. Gürtler, V. Saile, and P. Laporte, J. Chem. Phys. **91**, 1469 (1989).
[45] T. Oka, K. V. S. Rama Rao, J. L. Redpath, and R. F. Firestone, J. Chem. Phys. **61**, 4740 (1974).
[46] S. Arai, T. Oka, M. Kogoma, and M. Imamura, J. Chem. Phys. **68**, 4595 (1977).
[47] E. Zamir, D. L. Huestis, H. H. Nakano, R. M. Hill, and D. C. Lorents, IEEE J. Quantum Electron. QE **15**, 281 (1979).
[48] K. Kasama, T. Oka, S. Arai, H. Kurusu, and Y. Hama, J. Phys. Chem. **86**, 2035 (1982).
[49] P. Moutard, P. Laporte, M. Bon, N. Damany, and H. Damany, Opt. Lett. **10**, 538 (1985).
[50] R. Sauerbrey, H. Eizenhöfer, V. Schaller, and H. Langhoff, J. Phys. B **19**, 2279 (1986).
[51] K. P. Killeen and J. G. Eden, J. Chem. Phys. **83**, 6209 (1985); **84**, 6048 (1986).
[52] M. N. Ediger and J. G. Eden, J. Chem. Phys. **85**, 1757 (1986).
[53] E. Audouard, P. Laporte, and H. Damany, J. Opt. Soc. Am. B **6**, 1284 (1989).
[54] O. Echt, M. C. Cook, and A. W. Castleman, J. Chem. Phys. **87**, 3276 (1987).
[55] P. M. Dehmer and S. T. Pratt, J. Chem. Phys. **88**, 4139 (1988).
[56] R. S. F. Chang, H. Horiguchi, and D. W. Setser, J. Chem. Phys. **73**, 778 (1980), and references therein.
[57] E. Audouard, P. Laporte, J. L. Subtil, and N. Damany, J. Chem. Phys. **89**, 6176 (1988), and references therein.
[58] F. Spiegelmann, M. C. Castex, and F. X. Gadéa, Chem. Phys. **145**, 173 (1990).
[59] B. Huron, J. P. Malrieu, and P. Rancurel, J. Chem. Phys. **58**, 5745 (1973).
[60] F. Spiegelmann and J. P. Malrieu, J. Phys. B **17**, 1249(1984).
[61] C. Y. Ng, D. J. Trevor, B. H. Mahan, and Y. T. Lee, J. Chem. Phys. **66**, 446 (1976).
[62] P. M. Dehmer and J. L. Dehmer, J. Chem. Phys. **69**, 125 (1978).
[63] R. Abouaf, B. A. Huber, P. C. Cosby, R. P. Saxon, and J. T. Moseley, J. Chem. Phys. **68**, 2406 (1978).
[64] S. T. Pratt and P. M. Dehmer, Chem. Phys. Lett. **87**, 533 (1982).
[65] C. E. Moore, Nat. Bur. Stand. (U. S.) **467**, (1952), Vol. II.
[66] W. Klopper and W. Kutzelnigg, Chem. Phys. Lett. **134**, 17 (1987).
[67] K. Jankowski and P. Malinowski, Phys. Rev. A **21**, 45 (1980).
[68] N. Conrad, W. Gieβl, C. Leisner, R. Tietz, and H. Langhoff, Z. Phys. **16**, 71 (1990).
[69] R. A. Aziz, Mol. Phys. **38**, 177 (1979).
[70] M. Krauss, R. M. Regan, and D. D. Konowalow, J. Phys. Chem. **92**, 4329 (1988).
[71] P. B. Foreman, A. B. Lees, and P. K. Rol (unpublished results).
[72] O. Dössel, H. Nahme, R. Haensel, and N. Schwentner, J. Chem. Phys. **79**, 665 (1983).
[73] D. C. Shannon and J. G. Eden, J. Chem. Phys. **89**, 6644 (1988).
[74] E. Audouard, P. Laporte, J. L. Subtil, and R. Reininger (to be published).